An aerial photograph of a tropical coastline. A dirt road curves along the edge of a lush green forest. In the foreground, a sandy beach is visible with several red umbrellas and a small building. The water is a vibrant turquoise color, transitioning to a deeper blue further out. In the background, there are more green hills and a small town on a peninsula.

**Numerical simulation of  
submarine groundwater discharge:  
a case study in Curaçao**

Roel Jacobs



**WAGENINGEN UR**

**Wageningen University and Research**

**Numerical simulation of submarine groundwater discharge:  
a case study in Curaçao**

**Master's Thesis**

Hydrology and Quantitative Water Management Group

**Roel Jacobs**

**Supervisors: Victor Bense, George Bier**

March 22, 2022

# Contents

	<b>Page</b>
<b>Abstract</b>	<b>ii</b>
<b>1 Introduction</b>	<b>1</b>
1.1 Context and motivation . . . . .	1
1.2 Research Objectives . . . . .	2
1.3 Research Questions . . . . .	2
1.4 Thesis Outline . . . . .	3
<b>2 Field site and data</b>	<b>4</b>
2.1 Field site . . . . .	4
2.1.1 Land use . . . . .	4
2.1.2 Climate . . . . .	4
2.1.3 Geology . . . . .	5
2.2 Data . . . . .	7
2.2.1 Digital elevation model . . . . .	7
2.2.2 Pumping tests . . . . .	7
2.2.3 Groundwater level measurements . . . . .	7
<b>3 Methods</b>	<b>8</b>
3.1 MODFLOW . . . . .	8
3.1.1 Theoretical background groundwater model . . . . .	8
3.1.2 Regional plan view model . . . . .	9
3.1.3 Parameter analysis . . . . .	11
3.1.4 Quantification of submarine groundwater discharge . . . . .	12
3.2 SEAWAT . . . . .	13
3.2.1 Theoretical background variable density groundwater model . . . . .	13
3.2.2 Cross-sectional model . . . . .	15
<b>4 Results</b>	<b>17</b>
4.1 Regional plan view model . . . . .	17
4.1.1 Groundwater flow . . . . .	17
4.1.2 Parameter analysis . . . . .	18
4.1.3 Quantification of outflow . . . . .	20
4.2 Cross-sectional model . . . . .	21
4.2.1 Cross-sectional area . . . . .	21
4.2.2 Variable density groundwater flow . . . . .	22
4.2.3 Submarine groundwater discharge . . . . .	25
<b>5 Discussion</b>	<b>26</b>
5.1 Regional plan view model . . . . .	26
5.2 Cross-sectional model . . . . .	27
5.3 Submarine groundwater discharge . . . . .	28
5.4 Recommendations . . . . .	29

---

<b>6 Conclusion</b>	<b>30</b>
<b>Acknowledgements</b>	<b>31</b>
<b>Bibliography</b>	<b>32</b>
<b>Appendices</b>	<b>36</b>
A Groundwater level measurement locations . . . . .	36
B Top of the regional plan view model . . . . .	37
C Bottom of the regional plan view model . . . . .	38
D Parameter analysis . . . . .	39
E Flow lines particles cross-section . . . . .	42

## Abstract

The coral reefs around Curaçao are severely threatened by a combination of human and natural impacts. The abundance of coral reefs around Curaçao showed a rapid loss of nearly 50% in the last four decades. Water pollution is assumed to be one of the main drivers of this coral degradation. An often neglected pathway of nutrient and pollutant input is by submarine groundwater discharge (SGD). This research will help to identify and quantify this groundwater outflow towards the coral reefs. A regional numerical groundwater model was established with MODFLOW in order to model steady state groundwater flow towards the sea. For this model density effects were neglected. Due to limited field data, different scenarios were simulated in order to approximate the value of the average outflow. The average outflow in Curaçao ranged from 0.07 - 0.21 m/d. About half of this flows into the bays, and the other half is discharged as SGD. Secondly, a cross-sectional groundwater model was simulated with SEAWAT. This model incorporates density-driven flow in a 2D cross-section. The density dependent flow, geology and model parameters affect the freshwater/saltwater interface and the outflow of the model. The groundwater levels in the regional plan view groundwater model, where density effects were neglected, are slightly overestimated. On the other hand, the total outflow is slightly underestimated. The amount of total outflow is comparable with other studies that quantified the SGD for karstic islands, although a combination of methods is preferred to capture the spatial and temporal variability of the SGD.

# 1 Introduction

## 1.1 Context and motivation

One of the oldest ecosystems in the world are coral reefs (Pandolfi, 2011). These tropical coral reefs are known for having the highest species diversity of all explored marine habitats on Earth (Moberg, Rönnbäck, 2003). Curaçao is surrounded by a coral reef with an aerial extent of 103 km<sup>2</sup> (Global Coral Reef Monitoring Network, 2014). This ecosystem has a large impact on the society and economy of Curaçao, because this coral reef provides opportunities for recreation, fishery and tourism. Moreover, the coral reef provides protection for the coastline against storm surge and flooding. However, the coral reefs around Curaçao are severely threatened by a combination of human and natural impacts (Estep et al., 2017). A study performed by the Waitt Institute investigated the abundance of coral reefs over the years in Curaçao. This study showed a rapid loss of nearly 50% of the coral cover in the last four decades (Estep et al., 2017). Marine pollution, by both human activities and natural processes, is assumed to be one of the main drivers of this coral degradation.

Coral reef ecosystems occur in low-nutrient shallow coastal waters. Terrestrial nutrients and pollutants can reach the sea through sewage pipes and runoff (Estep, 2017). An often neglected pathway of nutrient input is by submarine groundwater discharge (SGD) (Moosdorf et al., 2014). This flow can transport nutrients and pollution to the sea (Figure 1). SGD is defined as the flow of water from terrestrial aquifers to coastal waters on continental margins (Moore, 2010). This groundwater flux has a relative high nutrient concentration compared to seawater or surface water (Street et al., 2008; Moore, 2010). Therefore, it potentially contributes to a large increase in the nutrient budget of the coral reefs. A research program (SEALINK) is organised to investigate the current coral reef health and the possible sources of pollutants in the ocean of the Dutch Caribbean (Vermeij, 2019).

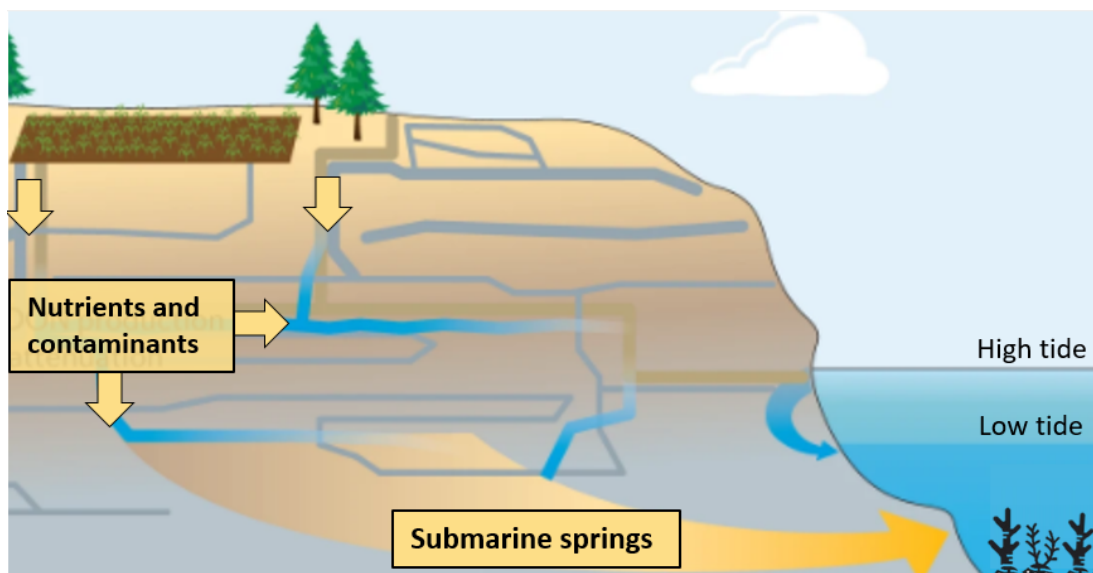


Figure 1: Submarine groundwater discharge by fractures and/or conduits in karstified carbonate rocks (Adapted from Santos et al. (2021))

In Curaçao, different geological formations are present which influences the storage and pathways of groundwater. Around the coast, multiple sequences of limestone terraces were formed (Beets,

MacGillavry, 1977). These karstified limestone formations are highly permeable due to the formation of conduit flows. When these conduits are connected to the sea, submarine groundwater discharge can occur. In Curaçao, it has been identified that nutrients and pollutants from these porous limestone formations end up in the marine environment (Estep et al., 2017). Furthermore, the groundwater quality and availability in coastal aquifers is also affected by seawater intrusion. The fresh groundwater in coastal aquifers mixes with seawater due to density differences. Within the salinity transition zone between fresh groundwater and saltwater re-circulation of seawater occurs. This variable density groundwater flow affects the submarine groundwater discharge (Prieto, 2005).

Abtmaier (1978) conducted a research about the hydrogeology of specific regions in Curaçao. In this study the potential of groundwater abstractions in selected areas was examined. He concluded that overpumping of the wells occurred in Curaçao from 1944 to 1960. In order to restore the groundwater levels, the government stopped groundwater pumping for domestic use in 1962 and the Shell oil refinery followed in 1973 (Louws et al., 1997). The expectation is that the cessation of the groundwater pumping has resulted in higher groundwater levels. As a result, the SGD has increased, due to a rise of the hydraulic gradient. However, no study has been conducted on the pathways of groundwater through the different geological formations. Moreover, the quantification of the SGD in Curaçao has not been determined in previous research. The heterogeneity of the geological formations makes it difficult to predict the groundwater flow based on directed measurements (Oberdorfer, 2003). On a regional scale, the freshwater flow can be simulated with a numerical model, which combines Darcy's law and the equation of conservation of mass. These numerical groundwater models are widely used to simulate SGD in other coastal aquifers (Hugman, 2017; Kaleris et al., 2002; Luoma et al., 2021).

## 1.2 Research Objectives

The goal of the SEALINK program is to assess how waterborne and land-derived inputs affect the growth and survival of the coral reefs in Curaçao. This research will help to identify the potential groundwater outflow towards these coral reefs. This will be investigated by modelling the hydraulic heads and groundwater flow through different geological formations towards the sea. The influence of the density driven flow on the outflow is examined by incorporating density effects in the model. The aim of this research is to simulate the groundwater flow and quantify SGD in Curaçao.

## 1.3 Research Questions

Based on these objectives for this study, research questions can be formulated. The main research question is:

Q1. What is the best description and quantification of submarine groundwater discharge on Curaçao?

Sub questions are:

Q1.1. What is the influence of the geological formations on the groundwater flow in Curaçao?

Q1.2. What is the impact of the model parameters on the uncertainty of the model output?

Q1.3. What is the influence of density driven flow on submarine groundwater discharge in Curaçao?

## **1.4 Thesis Outline**

Answers to these research questions will be presented in this report, which is organized the following way. In Chapter 2, the study area is described with regard to the geology, land use and climate of Curaçao. In addition, the meteorological and hydrogeological data are explained in this section. In Chapter 3, the numerical groundwater models are described and model choices are elucidated. In Chapter 4, the results from the regional plan view model and the cross-sectional model are explained. Moreover, the groundwater outflow will be quantified. In Chapter 5, the use of the groundwater models is discussed and recommendations for further research are provided. The final chapter will present the conclusions of this study.



## 2 Field site and data

### 2.1 Field site

The main island of Curaçao covers 444 km<sup>2</sup> and is located  $\pm 70$  km north of the Venezuelan coast of South America. Curaçao is geographically located between 11-12 ° N and 69-70° W. In general, the landscape is rugged and rocky. The highest point in Curaçao is the Christoffelberg (372 m), located at the north-west end of the island (Figure 2). Willemstad is the capital of Curaçao.

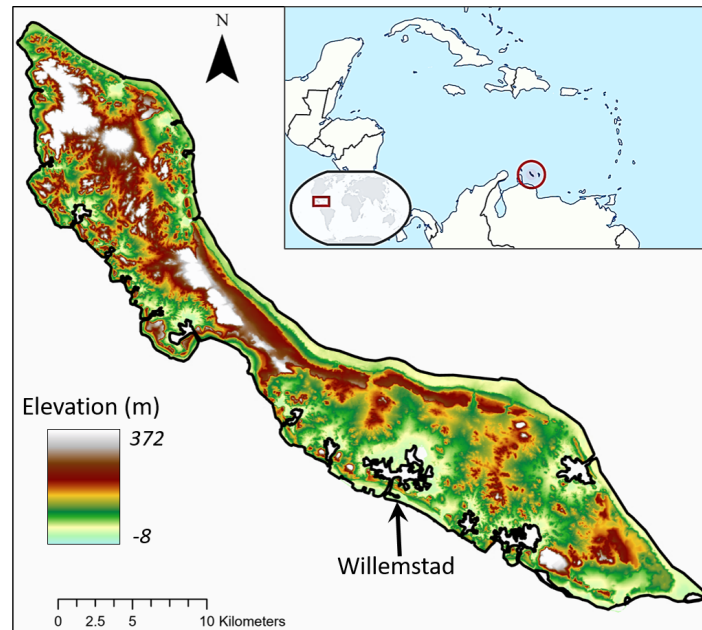


Figure 2: Study area, with elevation map of Curaçao.

#### 2.1.1 Land use

The city of Willemstad is located in the eastern part of the island. This urban area accounts for around 10% of the occupation of the island (De Vries, 2000). Small scale agriculture is only restricted to a few small areas. Due to water shortage most of the year, only areas with the presence of aquifers are suitable for small scale agriculture. The vegetation on Curaçao is adapted to the semi-arid conditions. Therefore, it consists of several species of cactus, dry woodland and dry grasses (Werger et al., 2016). Furthermore, several inland bays are situated in Curaçao. Some of these bays are densely fringed by mangroves (Debrot, Wells, 2008).

#### 2.1.2 Climate

Curaçao has a tropical semi-arid climate with a mean annual precipitation of 574 mm (De Vries, 2000). The intensity of the precipitation is highly variable and is influenced by a wet and dry season. The rainy season runs from October to December, whereas the dry season occurs from February to May (Figure 3). Heavy showers occur mainly during the rainy season (De Vries, 2000). Curaçao is characterised by tropical daytime temperatures ranging from 28 to 31 degrees Celsius. The highest mean temperature occurs in the month September. The high temperatures in combination with strong trade winds causes high evapotranspiration rates (85-95% of the precipitation). Only 5% of

the precipitation is recharged to the aquifers in Curaçao, because a large amount of water is lost due to evapotranspiration (De Vries, 2000). Precipitation with a moderate intensity infiltrates in the soil. Only episodic surface runoff events occur for precipitation with an extreme intensity (Den Haan et al., 2016). However, the dominant evapotranspiration rate creates a water shortage most of the year. Therefore, no perennial rivers or streams are present in Curaçao.

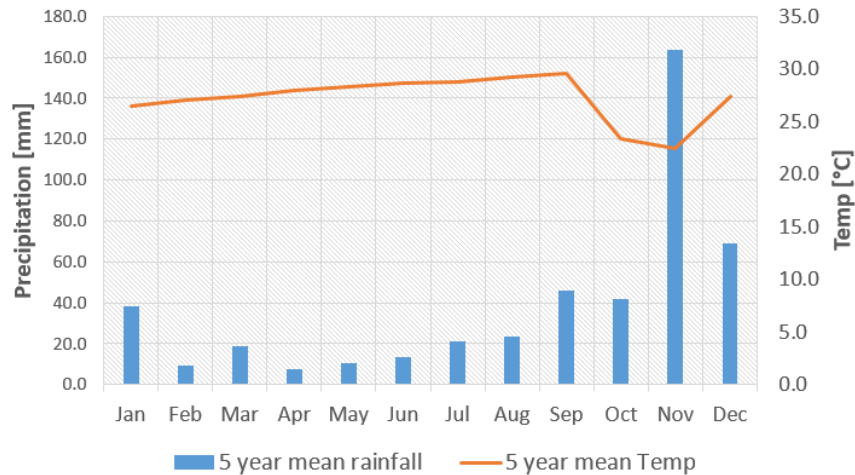


Figure 3: Climate Curaçao (Meteorological Department Curaçao). The 5 year average is measured in the period 2013-2017 for the weather station Hato Airport.

### 2.1.3 Geology

As described in the introduction, the geology on Curaçao features amongst others limestone formations. The geology mainly consists of volcanic and sedimentary materials. The temporal sequence of the geology is described in Figure 4. The geology and cross-sections are shown in Figure 5. The four exposed main geological formations on Curaçao are described below:





<b>Quaternary</b> (2.58 – 0 Ma)		Limestone Terraces
<b>Neogene</b> (23.03 – 2.58 Ma)		Seroe Domi Formation
<b>Paleogene</b> (66.0 – 23.03 Ma)		Mid Curacao Formation Knip Group
<b>Cretaceous</b> (145.0 – 66.0 Ma)		Curacao Lava Formation

Figure 4: temporal sequence of the main geological formations.

#### *Curaçao Lava Formation*

The NW and SE part of the island consists of two large anticlines of the Curaçao Lava Formation. This geological formation is formed due to strong magmatic activity during the Cretaceous. It is characterised by a more than 1000m thick monotonous succession of basalts. The toplayer of the basaltic rocks is weathered. This weathered zone, with a depth varying between 8 and 20 m below the surface, can be considered as a unconfined aquifer (De Vries, 2000).

### *Knip Group*

The Knip Group is a non-homogeneous group of nine different formations, which were formed during the Eocene (De Vries, 2000). This formation consists of sedimentary rocks including mainly silica-rich rocks and clastic sediments. The Knip Group is most abundant and exposed in the northwestern part of the island. The thickness of this formation is spatially variable over the island. In the northwestern part of the island it reaches a thickness of more than 2000 m. The central and southeastern part of Curaçao have a thickness of less than 100 m. This formation is presumed to be of late Senonian age (Beets, MacGillavry, 1977).

### *Mid Curaçao Formation*

Stratigraphically, the Knip Group is followed by the Mid Curaçao formation. This formation was formed during the Danian. The Mid Curaçao Formation is a turbidite sequence which consists of sandstones, siltstones, conglomerates and shales. This formation attains a thickness of at least 1000 m in the central part of the island.

### *Limestone Formation*

Hereafter, the tectonic rise in the Neogene and eustatic sealevel movements in the Quaternary resulted in the formation of carbonate rocks. This limestone formation can be divided in two units. Slow discontinuous emersion in the early-Neogene resulted in the formation of Seroe Domi Deposits. This formation consists of seaward dipping (between 15 - 25°) limestones (Beets, MacGillavry, 1977). The combination of tectonic rise and eustatic sealevel movement in the Quaternary resulted in the formation of limestone terraces around the coast (Beets, MacGillavry, 1977). The limestone formations are hosting karst features, which creates highly permeable solution conduits. This makes the hydrogeology complex in these areas (Van Sambeek et al., 2000). This is due to the fact that the determination of the conduit network is unknown (Bakalowicz, 2005).

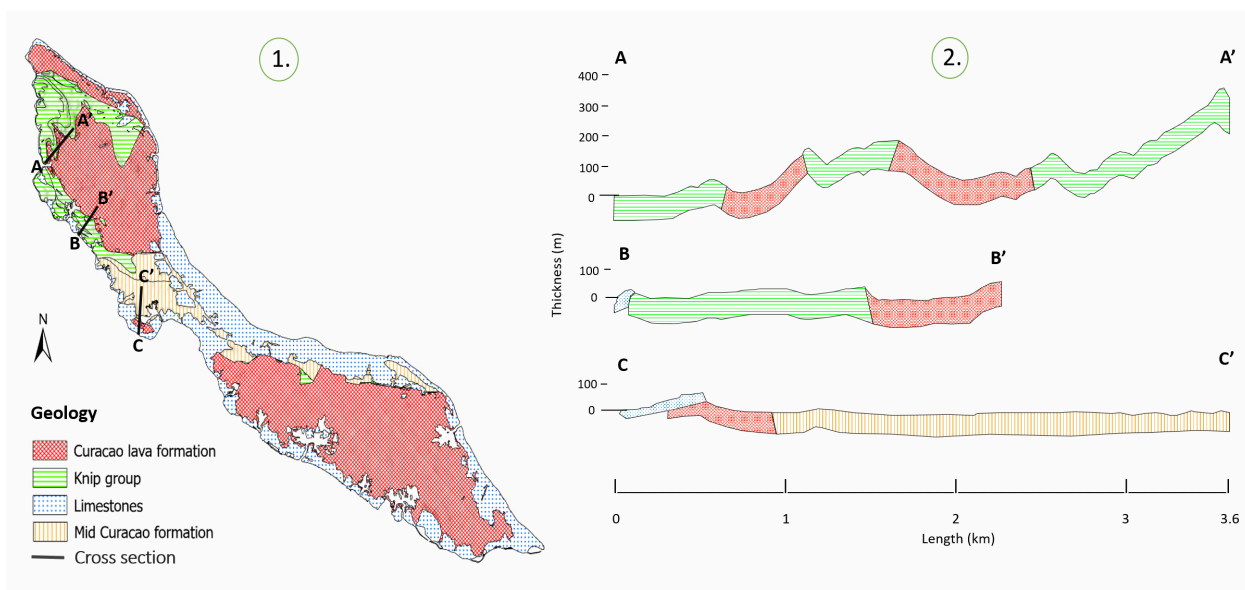


Figure 5: Geology (1) + cross sections (2) modified from (Beets, MacGillavry, 1977)

## 2.2 Data

### 2.2.1 Digital elevation model

A Digital Elevation Model (DEM) was provided by CARMABI (The Caribbean Research and Management of Biodiversity). This DEM has a resolution of 10 m x 10 m and covers the entire island. The topographic surface of Curaçao is visualised in Figure 2. In addition, CARMABI supplied a digitised version of the geology map composed by Beets (1972).

### 2.2.2 Pumping tests

During the study of Abtmaier (1978) 48 wells were drilled in different geological formations. The boreholes were drilled to a depth of 10 to 62 meters and contain a lithological description. This information was used as a background for the geology of Curaçao. Moreover, in this study 45 pumptests were conducted in different drainage catchments to calculate the hydraulic characteristics in different geological formations. From these pumping tests the transmissivity and specific yield were obtained. The hydraulic conductivity was calculated by dividing the transmissivity by the depth of the well. In table 1, the average transmissivity, hydraulic conductivity and specific yield of the four main geological formations are shown. No values were obtained for the limestone formations, because these boreholes were pumped dry very quickly. Input data about the hydrogeological parameters of the limestone formation were obtained from similar geological formations (Domenico et al., 1998; Whitaker, Smart, 1997).

Table 1: Average hydrogeological parameters of different geological formations. 31 pumping tests were conducted in the Curaçao Lava Formation, 8 in the Knip Group and 3 in the Mid Curaçao Formation.

<i>Geology</i>		<b>Transmissivity</b> <i>m<sup>2</sup>/d</i>	<b>Hydraulic conductivity</b> <i>m/d</i>	<b>Specific yield</b> <i>%</i>
<b>Curaçao Lava Formation</b>	<i>Average</i>	121.1	6.1	1.5
	<i>Standard deviation</i>	96.5	6.3	3.2
	<i>Range</i>	1.6-341	0.06-22	0.02-22
<b>Knip Group</b>	<i>Average</i>	22.5	0.63	4.4
	<i>Standard deviation</i>	26.7	0.85	4
	<i>Range</i>	1.0-79	0.03-2.2	0.09-14
<b>Mid Curaçao Formation</b>	<i>Average</i>	7.5	0.31	4
	<i>Standard deviation</i>	5.4	0.15	2.2
	<i>Range</i>	1.3-15	0.16-0.5	1.4-7.5

### 2.2.3 Groundwater level measurements

Several groundwater level measurements were conducted for the SEALINK project. The measurements were obtained between October and December 2021. 63 wells were spatially distributed over the island (Appendix A). The level of the groundwater was measured below the surface. This level was converted to the groundwater level compared to sea level. Moreover, at 49 locations the electrical conductivity (EC) was measured. The change of the EC over depth was measured in mS/cm. These EC profiles ranged from the groundwater level until approximately 30 meters below the surface.

### 3 Methods

The outflow of groundwater towards the sea was evaluated in two steps:

1. First, a regional plan view groundwater model was created by using MODFLOW. For this model, density effects are neglected and a coarser grid was used.
2. The second step was to generate a cross-sectional groundwater model using SEAWAT. Hereby, density effects are incorporated and a finer grid was used. Due to the computational demand of the SEAWAT model, this approach was limited to evaluate cross-sections.

For this study, first, the theoretical background of the groundwater model MODFLOW is described, in which the mathematical calculations of the model are explained. Secondly, the setup of this model is described. Hereby, the choices for discretisation, initial and boundary conditions, simulation period, hydrogeological parameters and sources/sinks are explained. After this, the theoretical background and model setup of the SEAWAT model is explained.

#### 3.1 MODFLOW

##### 3.1.1 Theoretical background groundwater model

MODFLOW is a widely used to simulate the three-dimensional groundwater flow and is developed by the United States Geological Survey (USGS) (McDonald, Harbaugh, 1988). The modelling was executed with Groundwater Modeling System (GMS) software. The software of GMS is a widely applied graphical user interface for groundwater models, such as MODFLOW, SEAWAT and MT3DMS (Aghlmand, Abbasi, 2019). The strength of this software lies within the integration with Geographic Information System (GIS). The groundwater model was based on a finite volume approach. Groundwater flow through a porous media can be described with Darcy's law. This law states that the discharge rate  $q$  is proportional to the hydraulic conductivity and the gradient in hydraulic head, which can be written as:

$$q_i = -K_{ij} \frac{\partial h}{\partial x_j} \quad (1)$$

The three-dimensional groundwater flow of constant density in a porous aquifer may be described by the partial-differential equation ((Konikow et al., 2006)):

$$\frac{\partial}{\partial x} (K_{xx} \frac{\partial h}{\partial x}) + \frac{\partial}{\partial y} (K_{yy} \frac{\partial h}{\partial y}) + \frac{\partial}{\partial z} (K_{zz} \frac{\partial h}{\partial z}) + W = Ss \frac{\partial h}{\partial t} \quad (2)$$

Where  $K_{xx}$ ,  $K_{yy}$  and  $K_{zz}$  are values of hydraulic conductivity along the x, y, and z coordinate axes [ $L T^{-1}$ ]. The potentiometric head is characterised by  $h$  ( $L$ ).  $W$  is the volumetric flux per unit volume (representing sources and/or sinks) [ $T^{-1}$ ]. Moreover,  $Ss$  is the specific storage [ $L^{-1}$ ] and  $t$  is time [ $T$ ]. The groundwater flow takes place in a heterogeneous and anisotropic environment. Therefore, the axes of the hydraulic conductivity are aligned with the coordinate directions.

In order to solve this three-dimensional groundwater flow equation (2), the equation will be described in a finite difference form. The groundwater flow between cells is determined by the hydraulic conductance and the head difference. The flow is considered positive if it is entering the cell. The flow between cells is called the internal flow (Figure 6a). This internal flow for a one-dimensional

steady-state case from node m to node n with cross-sectional area  $\Delta w$  (width) and  $\Delta v$  (height) can be described by:

$$Q_{n,m} = K_{n,m} * \Delta w_{n,m} * \Delta v_{n,m} \frac{h_m - h_n}{L_{n,m} - L_{m,n}} \quad (3)$$

Where  $K_{n,m}$  is the length-weighted harmonic mean of the hydraulic conductivity of the two blocks. This hydraulic conductivity can be calculated for an aquifer consisting of n blocks by:

$$K_{n,m} = \frac{\sum_{i=1}^n L_i}{\sum_{i=1}^n \frac{L_i}{K_i}} \quad (4)$$

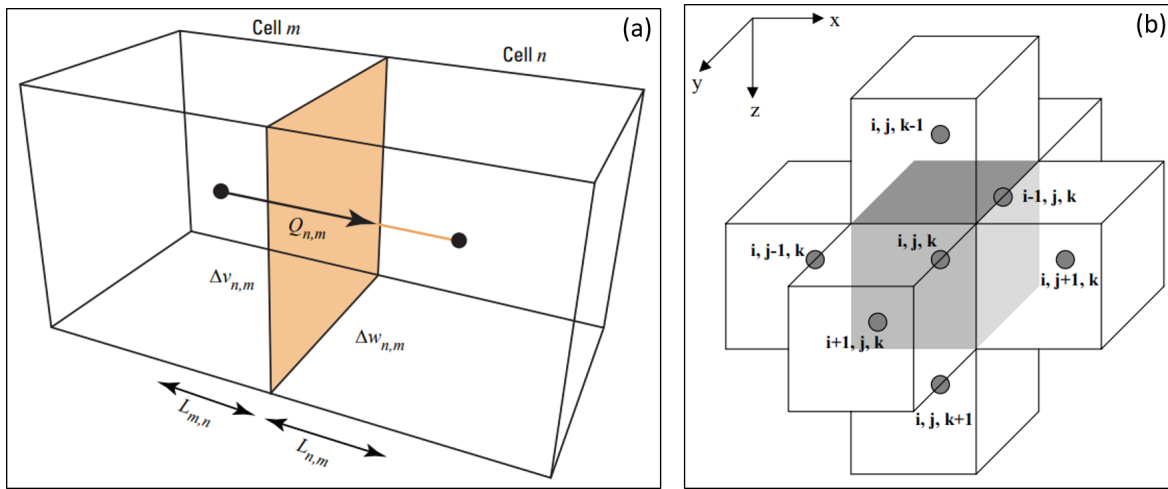


Figure 6: Flow between cells in MODFLOW. Whereby Figure 6a shows the internal flow for a one-dimensional steady state case (Langevin et al., 2017), and Figure 6b a finite-volume grid in x,y,z-direction (Zheng et al., 1999)

The partial differential equation (2) can be transformed into a finite difference form in three dimensions for a cell (i,j,k) (Figure 6b). Where the head is unknown for  $h_{i,j,k}^{n+1}$  at timestep  $t^{n+1}$  and where the head  $h_{i,j,k}^n$  at previous timestep  $t^n$  is known. The differential equation of the internal and external fluxes can be described by:

$$\begin{aligned} & \frac{K_{xx} |_{i+1/2,j,k} \cdot (h_{i+1,j,k}^{n+1} - h_{i,j,k}^{n+1}) - K_{xx} |_{i-1/2,j,k} \cdot (h_{i,j,k}^{n+1} - h_{i-1,j,k}^{n+1})}{\Delta x^2} + \\ & \frac{K_{yy} |_{i,j+1/2,k} \cdot (h_{i,j+1,k}^{n+1} - h_{i,j,k}^{n+1}) - K_{yy} |_{i,j-1/2,k} \cdot (h_{i,j,k}^{n+1} - h_{i,j-1,k}^{n+1})}{\Delta y^2} + \\ & \frac{K_{zz} |_{i,j,k+1/2} \cdot (h_{i,j,k+1}^{n+1} - h_{i,j,k}^{n+1}) - K_{zz} |_{i,j,k-1/2} \cdot (h_{i,j,k}^{n+1} - h_{i,j,k-1}^{n+1})}{\Delta z^2} - W |_{i,j,k} = S_s |_{i,j,k} \cdot \frac{h_{i,j,k}^{n+1} - h_{i,j,k}^n}{t^{n+1} - t^n} \end{aligned} \quad (5)$$

### 3.1.2 Regional plan view model

For this study, the version MODFLOW-2000 was used to simulate the groundwater flow for Curaçao. This regional plan view groundwater model is constructed with several packages. MODFLOW facilitates a series of packages that perform a specific task. Required packages were the Basis (BAS), Discretisation (DIS), Preconditioned Conjugate-Gradient (PCG) and Output Control (OC) packages. The

internal flow package chosen for this study is the Layer Property Flow (LPF) package. In this package, the hydraulic properties are defined. Other packages used are Recharge (RCH), Time-Variant Specified-Head (CHD) and Head-Observation (HOB) packages and are explained below.

#### *Flow domain and boundary conditions*

This regional plan view groundwater model covers the entire island of Curaçao. In this numerical model, one boundary condition was applied. The Caribbean Sea was defined as the specified head boundary having a constant head equal to the average sea level of 0 m (Figure 7). This Dirichlet condition was defined with Time-Variant Specified Head (CHD) package. There are no lakes, rivers or other natural freshwater sources on Curaçao. Therefore, this was not included in the determination of boundary conditions. The starting heads were equal to the top elevation. Due to lack of data from the study area, as well as the complexity of the hydrogeological system, the flow was assumed to be in steady state conditions.

#### *Discretisation*

This groundwater model contains a large variation in hydraulic properties. To reduce the effect of this heterogeneity, the flow domain is approximated with a cell size of 100 x 100 m. These cells consist of the same regular rectangles.

#### *Schematisation*

As described in Chapter 2.1.3, the geological formations on Curaçao are characterised by thick formations of bedrock with a weathered top layer. Accordingly, the groundwater flow model was generalised as a single-layered aquifer representing the weathered top layer. Therefore, the Layer Property Flow (LPF) package consists of 1 layer. The vertical flux in this groundwater model was assumed to be zero. A Digital Elevation Model (DEM) was integrated in MODFLOW. This served to capture the top of the first layer and the perimeter of Curaçao. The bottom of the layer is defined by the bottom of the boreholes of the study of Abtmaier (1978). Moreover, the bottom for the cells at the boundary of the model have a value of -20 m below sea level. The area between the boreholes was estimated by linear interpolation of the boreholes and boundary. Therefore, the thickness of the layer depends on the top elevation and the depth of the boreholes. In Appendix B and C the top and bottom of the model are shown. The thickness of the groundwater model varies between 5 and 360 m.

The determination of the hydraulic conductivity was based on a digitised version of the surface geological map (Beets, MacGillavry, 1977). The geological regions were defined using polygons and are visualised in Figure 7. The hydraulic conductivity of each geological formation was based on pumping tests conducted by Abtmaier (1978). Table 1 in Chapter 2.2.2 indicates the average hydraulic conductivity for the Curaçao lava formation, Knip group and Mid-Curaçao formation. For the limestone formation an average hydraulic conductivity of 15 m/d is assumed (Domenico et al., 1998; Whitaker, Smart, 1997). These average values for the hydraulic conductivity are implemented in the Layer Property Flow (LPF) package.

As described in section 2.1.2., the recharge to the aquifers in Curaçao is 5% of the precipitation, which is equal to 28.7 mm/year. In this study, this amount of direct recharge is distributed constantly over the entire island. The Recharge (RCH) package is used to define the recharge flux. This recharge flux was only applied on the top layer.

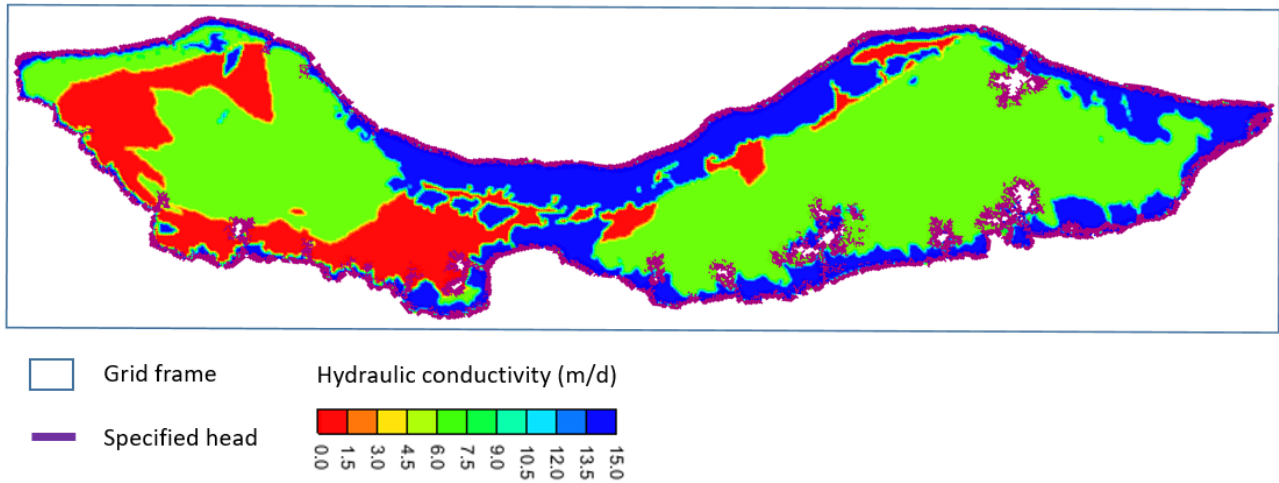


Figure 7: The grid frame of the regional plan view model, with a specified head as boundary condition. The geological formations are visualised with a specified hydraulic conductivity.

### 3.1.3 Parameter analysis

The input parameters of the groundwater model were obtained from fieldwork and literature. However, this groundwater model has to deal with a high level of uncertainty. Even well-calibrated groundwater models are associated with a significant amount of uncertainty (Mugunthan, Shoemaker, 2006). Especially the input parameters hydraulic conductivity and recharge are vulnerable to uncertainty (El Mezouary, El Mansouri, 2021). Due to the fact that there was limited calibration data available, a stochastic modeling approach was used to estimate the probability of certain outcomes and to deal with this uncertainty (Liu et al., 2005). This stochastic modeling approach was performed with parameter zonation method Latin Hypercube. For each parameter a minimum value, maximum value, mean and standard deviation was defined (Table 2). For the Latin Hypercube method the number of simulations is specified. A larger number of simulations indicate a greater confidence that more outcomes are explored. The total number of simulations is determined by the product of the number of segments for each parameter. Therefore, the groundwater model generated for two segments per parameter:  $2^5 = 32$  simulations.

Table 2: Parameter distribution, where  $K_x$  is the hydraulic conductivity (m/d) of the geological formations (Knip = Knip Group, CLF = Curaçao Lava Formation, Mid = Mid Curaçao Formation) and the other parameter is the recharge to the aquifer (m/d).

Parameter	Average	Min	Max	St.Dev
$K_{limestone}$	15	0.1	2000	20
$K_{Knip}$	0.63	0.03	2.17	0.85
$K_{CLF}$	6.1	0.06	22	6.3
$K_{Mid}$	0.31	0.16	0.45	0.15
Recharge	0.000079	0.000039	0.000629	1.95

The Head-Observation package (HOB) is used to specify the observations of hydraulic heads. For each simulation a mean absolute error and a root mean square error is calculated. The mean absolute error calculates the mean of the absolute error values between the observations and calculated heads.



Lower values for the mean absolute error means a better fit between the observed and calculated heads. The mean absolute error (MAE) is calculated by the following equation (Aghlmand, Abbasi, 2019):

$$MAE = \frac{1}{n} \sum_{i=1}^n |(h_o - h_c)_i| \quad (6)$$

Where  $n$  is the number of observations,  $h_o$  is the observed head ( $L$ ) and  $h_c$  is the calculated head ( $L$ ). The root means square error is calculated by the average of the squared error for the observations and taking the square root of this average. The root mean square error (RMSE) is calculated by the following equation (Aghlmand, Abbasi, 2019):

$$RMSE = \left[ \frac{1}{n} \sum_{i=1}^n (h_o - h_c)_i^2 \right]^{0.5} \quad (7)$$

### 3.1.4 Quantification of submarine groundwater discharge

The total outflow was quantified for the groundwater that flows towards the sea and the bays. The distinction between the outflow towards the bays and the sea was useful for the quantification of the SGD. The boundary of the groundwater model was appointed as a specific zone budget (Figure 8). The outflow towards the sea was specified as zone budget 1. The outflow for this zone budget was determined as SGD, because this outflow is directly linked to the sea. Zone budget 2 was defined as the outflow towards the bays. This zone budget is the minor part of the perimeter of the island compared to zone budget 1. The outflow for zone budget 2 is not determined as SGD, because these bays are defined as separate areas.

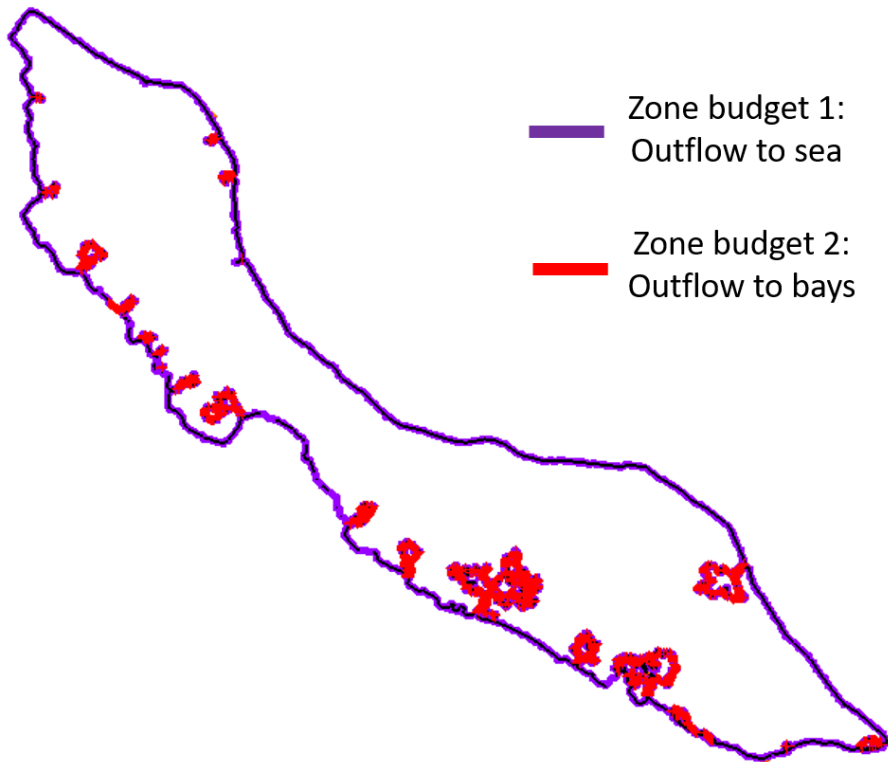


Figure 8: Definition of zone budgets distinguishing between outflow towards the sea (purple) and towards the bays (red).

## 3.2 SEAWAT

### 3.2.1 Theoretical background variable density groundwater model

The SEAWAT program was developed by Guo, Langevin (2002). This program simulates three-dimensional variable-density groundwater flow for transient conditions in a porous media. SEAWAT combines MODFLOW and MT3DMS (Zheng et al., 1999) into a single program that solves the coupled groundwater flow and solute transport. The MODFLOW program is based on the assumption of a constant fluid density. However, in coastal aquifers, the groundwater quality and availability is affected by the interaction of groundwater and seawater. These variable density conditions also affects the hydraulic heads of the aquifer. For two points with equal pressure at the same elevation, different hydraulic heads can be found for different water densities (Figure 9). Therefore, the equivalent fresh water head  $h_f [L]$  is taken into account and is defined as:

$$h_f = \frac{P_N}{\rho_f g} + Z_N \quad (8)$$

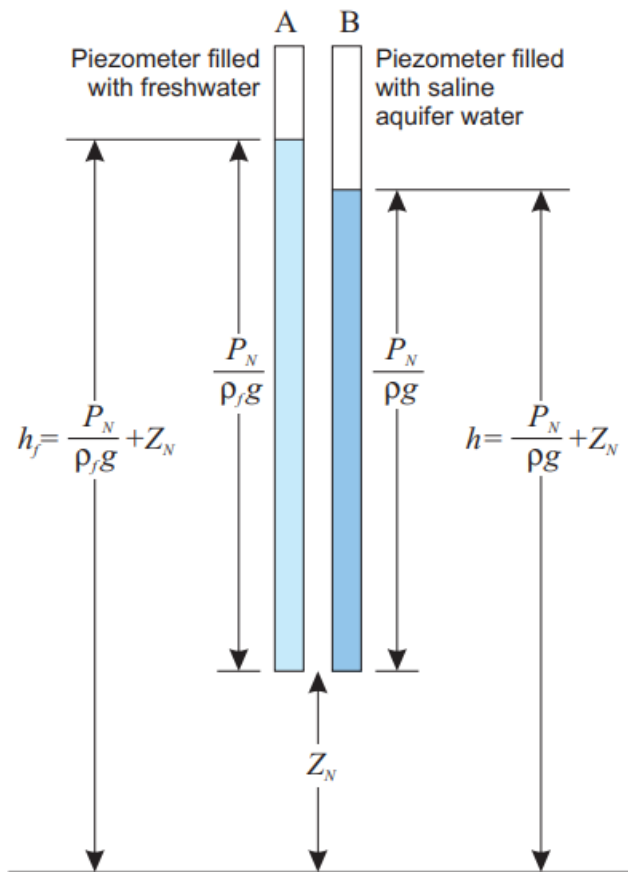


Figure 9: Density effect piezometer (Guo, Langevin, 2002)

where  $h_f$  is the equivalent fresh water head  $[L]$ ,  $P_n$  is the pressure at point N  $[ML^{-1}T^{-2}]$ ,  $\rho_f$  is the density of freshwater which is equal to  $1000 \text{ kg m}^{-3}$ ,  $g$  is the gravitational acceleration  $[LT^{-2}]$  and  $Z_N$  is the elevation  $[L]$ . For the  $x$  and  $y$ -direction Darcy's law applies for the specific discharge of groundwater. However, this variable density groundwater flow has an effect on the specific discharge in the  $z$ -direction. The specific discharge in the upward coordinate direction ( $z$ ) is expressed by:

$$q_z = -\frac{k_z}{\mu} \left[ \frac{\partial P}{\partial z} + \rho g \right] \quad (9)$$

where  $q_z$  is the specific discharge [ $LT^{-1}$ ],  $k_z$  is the intrinsic permeability [ $L^2$ ],  $\mu$  is the dynamic viscosity [ $ML^{-1}T^{-1}$ ].

This specific discharge can be solved by using the partial differential equation for variable density groundwater flow. Therefore, Equation 9 is solved for  $p$ , viscosity differences are neglected and the hydraulic conductivity tensor  $K_f$  [ $LT^{-1}$ ] is initiated.  $K_f$  is formulated by  $K_f = k\rho g/\mu_f$  (Senger, Fogg, 1990). Darcy's law in terms of equivalent freshwater head is expressed by:

$$-k_f \left[ \frac{\partial h_f}{\partial z} + \frac{(\rho - \rho_f)}{\rho_f} \right] = \rho S_s \frac{\partial h_f}{\partial t} + \theta \frac{dp}{dC} \frac{dC}{dt} - \rho_{ss} q_{ss} \quad (10)$$

where  $S_s$  is the specific storage [ $L^{-1}$ ],  $\theta$  is the effective porosity [-],  $C$  is the concentration [ $ML^{-3}$ ],  $\rho_{ss}$  is the density of the sink or source [ $ML^{-1}$ ],  $q_{ss}$  is the specific discharge of the sink or source term [ $T^{-1}$ ] and  $t$  is the time [ $T$ ].

The previous partial differential equation only describes the groundwater flow. However, to simulate the density dependent flow, the transport of solute mass in the aquifer is required. MT3DMS is used to simulate the solute transport. The fate and transport of the solute mass in three-dimensional, transient groundwater flow systems can be expressed by:

$$\frac{\partial(\theta C)}{\partial t} = \frac{\partial}{\partial x_i} (\theta D_{ij} \frac{\partial C}{\partial x_j}) - \frac{\partial}{\partial x_i} (\theta v_i C) + q_{ss} C_{ss} \quad (11)$$

where  $D$  is the hydrodynamic dispersion tensor [ $L^2 T^{-1}$ ],  $v$  is the pore water velocity [ $LT^{-1}$ ] and  $C_{ss}$  is the solute concentration of water from sources or sinks [ $ML^{-3}$ ].

This partial differential equation is numerically solved with a third-order TVD scheme. The advantage of this TVD scheme is the capability to solve the advection term independently of other terms. The specific discharge  $q$  is calculated by multiplying  $\theta$  and  $v$ . The three-dimensional transport equation considering advection alone is solved numerically with an explicit finite-difference algorithm and can be expressed with:

$$\theta_{i,j,k} \frac{C_{i,j,k}^{n+1} - C_{i,j,k}^n}{\Delta t} = - \frac{q_{xi,j+1/2,k} C_{i,j+1/2,k}^n - q_{xi,j-1/2,k} C_{i,j-1/2,k}^n}{\Delta x_j} - \frac{q_{yi+1/2,j,k} C_{i+1/2,j,k}^n - q_{yi-1/2,j,k} C_{i-1/2,j,k}^n}{\Delta y_i} - \frac{q_{zi,j,k+1/2} C_{i,j,k+1/2}^n - q_{zi,j,k-1/2} C_{i,j,k-1/2}^n}{\Delta z_k} \quad (12)$$

MODFLOW and MT3DMS are coupled in SEAWAT. This coupling between flow and transport is visualised in Figure 10. For this coupling, the stress periods are divided into timesteps. The specific discharge was calculated from the results of the groundwater flow simulation at time  $t_n$  and was proceeded to the transport equations to represent the groundwater flow over time interval  $\Delta t_n$ .

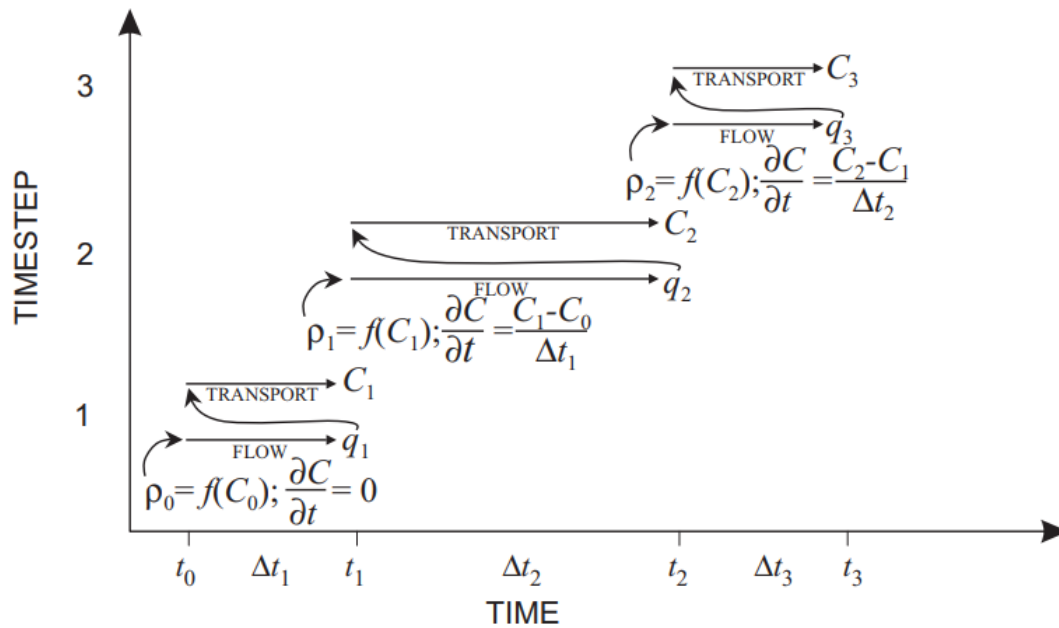


Figure 10: Coupling MODFLOW and MT3DMS (Guo, Langevin, 2002)

### 3.2.2 Cross-sectional model

Several packages from MODFLOW and MT3DMS were used to simulate the density dependent flow of groundwater in SEAWAT. For this cross-sectional model, the same required packages are used as in Chapter 3.1.2 (BAS, DIS, PCG and OC). Moreover, the Layer Property Flow package (LPF) was chosen to as internal flow package. In addition, other MODFLOW packages used were Layer Property Flow (LPF), Recharge (RCH) and Time-Variant Specified Head (CHD) packages. For MT3DMS, several other packages were involved to simulate the solute transport. The packages used for MT3DMS were Basic Transport (BTN), Generalized Conjugate Gradient Solver Pane (GCG), Advection (ADV) and Source/Sink Mixing (SSM).

#### *Flow domain and boundary conditions*

This cross-sectional groundwater model is located at a suitable cross-section perpendicular to the coastline of Curaçao. Within this cross-section the freshwater/saltwater interface is simulated. The location of this cross-section depends on the regional plan view model, because the groundwater flow should be parallel to the cross-section. Therefore, the effect of inflow over the boundaries is neglected. For this model, the Carribean Sea was also defined as the specified head boundary having a constant head equal to the average sea level of 0 m. This dirichlet condition was defined with Time-Variant Specified Head (CHD) package. The boundary on the other side of the cross-section is a no flow boundary. This boundary is located at the water divide of the regional plan view model. First a steady-state groundwater flow simulation was executed to simulate the initial conditions of the model. These initial conditions are used as starting heads for the density dependent groundwater flow. This density dependent groundwater flow was performed with SEAWAT for transient conditions.

#### *Discretisation*

This variable density flow model also contains a large variation in hydraulic properties. The cell size was reduced for this cross-sectional model. Therefore, the flow domain is approximated

with a cell size of 5 x 5 m in the x and z- direction. These cells consist of the same regular rectangles.

### *Schematisation*

The hydraulic conductivity of the different geological layers was based on the regional plan view model. The same average values for the hydraulic conductivity were used as input parameters for the cross-sectional model. The hydrogeological characteristics were defined by the Layer Property Flow package (LPF). The recharge was defined by the Recharge package (RCH). The average recharge flux is also based on the regional plan view model.

MT3DMS was used to simulate the solute transport. In the Basic Transport package (BTN) the stress period was defined. Moreover, the starting conditions were determined. The starting condition for the cross-section was a salt starting concentration of  $35 \text{ kg m}^{-3}$ . This concentration is equal to the salt concentration of seawater. On top of first layer a constant recharge flux was applied with a salt recharge concentration. This salt recharge concentration was obtained from the electrical conductivity (EC) depth profiles (Chapter 2.2.3.). The salt recharge concentration is defined based on the Source/Sink Mixing package (SSM). The same package was used to determine the salt concentration for the specified head boundary. The salt concentration for this constant head is equal  $35 \text{ kg m}^{-3}$  for the entire stress period. For the Advection package (ADV), a third order TVD scheme was used as solution scheme. This TVD scheme has the capability to solve the advection term independently of other terms.

## 4 Results

In this chapter, first, the results of the regional plan view model are described. Moreover, the parameter analysis determines the optimal input parameters for this model. The regional plan view model will also define the amount and direction of the total outflow. The results of this regional plan view model are used as input for the cross-sectional model. The selection of the location for the cross-sectional area is described in this section. In addition, the results of the variable density flow with corresponding freshwater/saltwater interface for this cross-section are explained. Finally, the SGD is quantified using the cross-sectional model.

### 4.1 Regional plan view model

#### 4.1.1 Groundwater flow

The entire model structure consists of a matrix of 147 rows x 603 columns x 1 layer. This layer contains spatially variable hydrogeological properties (Figure 7) and is variable in thickness. The cells are composed of the same regular rectangles. The total number of active cells for the entire island is 44369 with a cell size is 100 x 100 m. The simulated groundwater levels above mean sea level (MSL) are visualized in Figure 11.

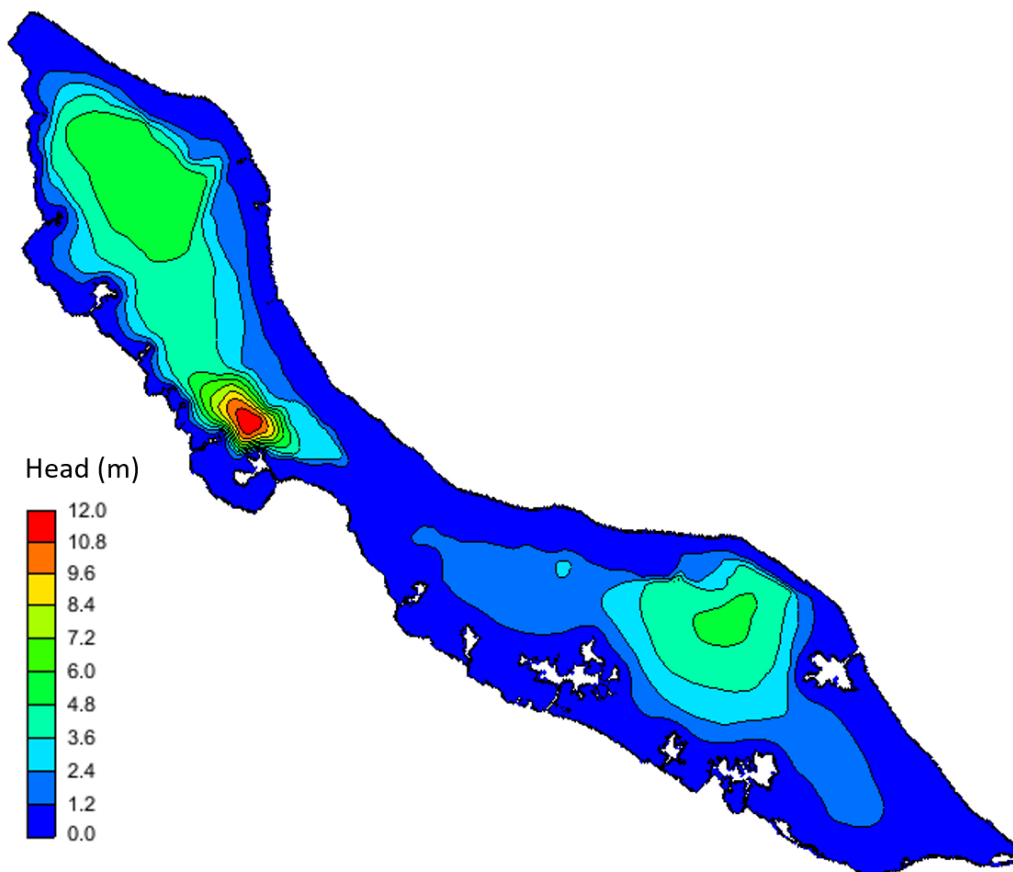


Figure 11: Simulated groundwater levels compared to mean sea level (M.S.L.)

Two large groundwater bulges are present at the northern and southern part of the island. In the middle of the island, the largest hydraulic heads are simulated. Shallow cells (10-30 m) in combination with the low hydraulic conductivity of the Mid Curaçao Formation (0.31 m/d) generate high groundwater

levels (10.8-12.0 m). Moreover, low hydraulic heads are present in the limestone formation along the coast (0.0-1.2 m), due to the high hydraulic conductivity of this formation (15 m/d). The general flow pattern is from the middle of the island towards the coast, due to the fact that water flows from high to low hydraulic heads. Another factor that affects the groundwater flow in Curaçao are the bays. These bays create notches in the distribution of the groundwater levels. This is caused by the specified head boundary condition around these bays. The flow budget is only influenced by the recharge and the outflow over the boundary condition. This flow budget of the regional plan view model is shown in table 3.

Table 3: Flow budget of regional plan view model

Source	Inflow <i>m<sup>3</sup>/d</i>	Outflow <i>m<sup>3</sup>/d</i>
Recharge	32269.2	0.0
Constant head	0.0	32269.4
Total	32269.2	32269.4

#### 4.1.2 Parameter analysis

The average values for the input parameters, obtained from pumping tests and literature, result in the simulated groundwater levels described in Chapter 4.1.1. However, the outcomes of the groundwater flow model are strongly based on the assumptions of the input parameters. The parameters from the four best model runs of the Latin Hypercube method are shown in Table 4.

Table 4: Input parameters from the four best model runs based on the comparison with observations.

Run	<i>Parameters</i>					<i>Comparison observations</i>	
	$K_{limestone}$ <i>m/d</i>	$K_{Knip}$ <i>m/d</i>	$K_{CLF}$ <i>m/d</i>	$K_{Mid}$ <i>m/d</i>	Recharge <i>m/d</i>	M.A.E. <i>m</i>	R.M.S.E. <i>m</i>
11	0.33	0.84	0.61	0.40	0.00005	10.26	15.92
15	2.93	0.50	2.50	0.40	0.00006	10.76	16.9
23	767.05	0.36	4.80	0.36	0.00013	10.76	17.15
31	70.63	0.95	4.01	0.30	0.00014	10.55	17.17

There is a large variation in the distribution of the parameters. The hydraulic conductivity of the limestone formation ( $K_{limestone}$ ) itself does not greatly affect the simulated hydraulic heads. This can be explained by the fact that both a value of 0.33 *m/d* and 767.05 *m/d* generate the lowest error of the model runs. The range of the hydraulic conductivity of the Mid Curaçao formation ( $K_{Mid}$ ) and Knip Group ( $K_{Knip}$ ) is small. Therefore, these parameters have less influence in the simulation of the groundwater levels.

Appendix D shows the results of all 31 model runs. The model runs are sorted from low to high Root Mean Square Error (R.M.S.E.). In general, model runs with a relatively large recharge flux ( $\geq 0.0002$  *m/d*) have a larger error. The combination of a large recharge flux ( $\geq 0.0002$  *m/d*) and low hydraulic conductivity values for limestone formations ( $K_{Limestone}$ :  $\leq 1$  *m/d*) and the Curaçao lava formation

( $K_{CLF} \leq 0.4 \text{ m/d}$ ) results in the largest errors.

In Figure 12, the simulated groundwater levels from the four model runs (table 4) are shown. There is a large variety in the distribution of the groundwater levels for the different model runs. This indicates that the input parameters are important for the model output. The hydraulic conductivity of the Curaçao Lava Formation ( $K_{CLF}$ ) and the Limestone Formation ( $K_{Limestone}$ ) are the most dominant for the distribution of the groundwater levels. If  $K_{Limestone}$  is significantly larger than  $K_{CLF}$ , a groundwater bulge in the middle and southern part of the island is formed (Run 23 and Run 31). If  $K_{CLF}$  is significantly larger than  $K_{Limestone}$ , a groundwater bulge in the middle and northern part of the island is formed. When  $K_{Limestone}$  and  $K_{CLF}$  are approximately equal then a groundwater bulge forms in the northern and southern part of the island (Run 11 and Run 15). The magnitude of the recharge flux and the hydraulic conductivity determine the height of the groundwater levels. However, the distribution of the groundwater levels consist of the same pattern.

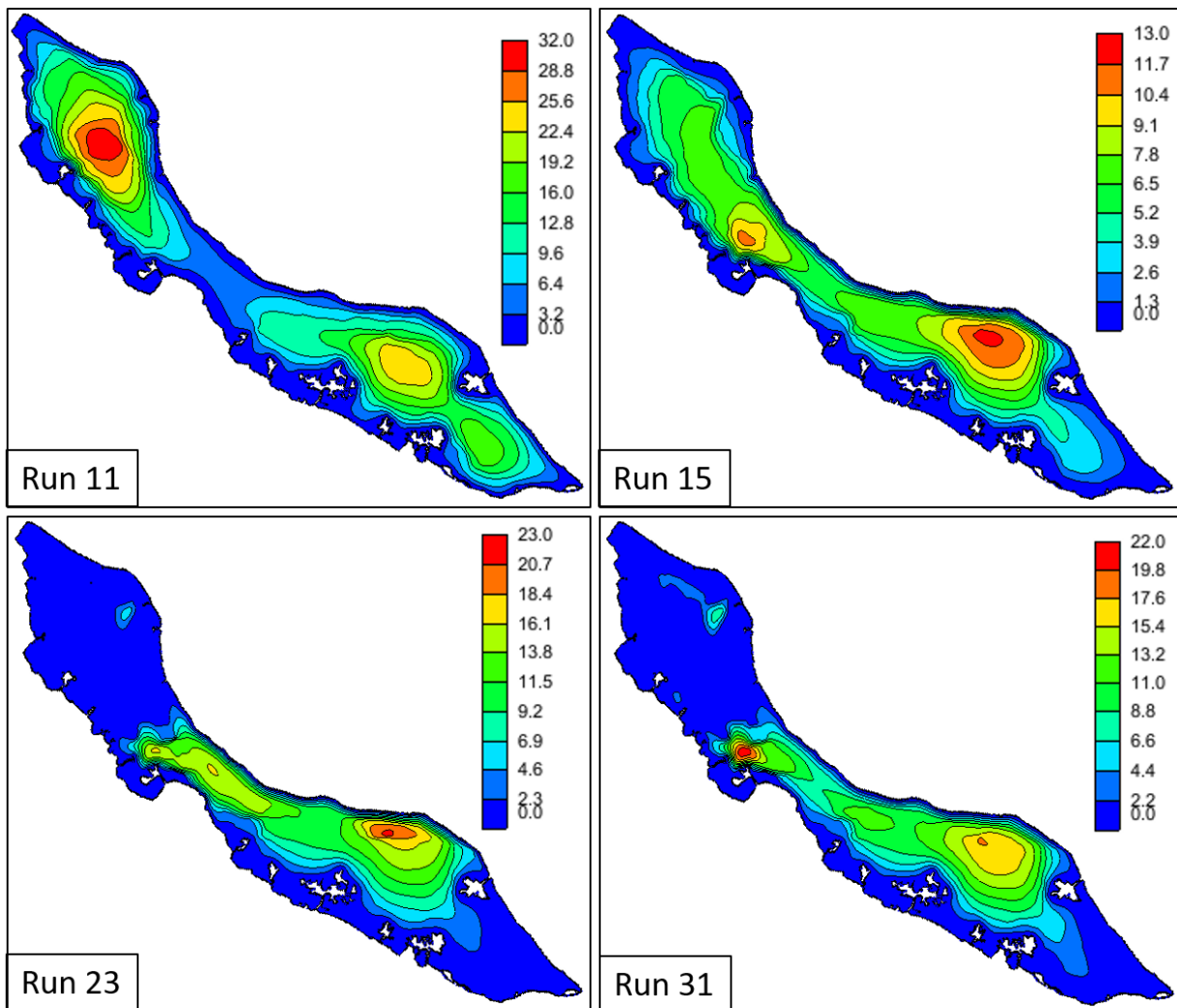


Figure 12: Effect input parameters for four different model runs (11, 15, 23, 31) with the lowest Root Mean Square Error (R.M.S.E.).



### 4.1.3 Quantification of outflow

The total outflow over the boundary condition is simulated for the four model runs shown in Table 4. The amount of the outflow towards the bays and the sea is visualised in Figure 13. The amount of outflow varies substantially ( $0.07\text{-}0.21\text{ m/d}$ ) between the different model runs. The lower recharge values result in a lower outflow over the boundary. Therefore, the outflow for model run 23 and model run 31 is two times larger compared to model run 11 and model run 15. However, The distribution of the outflow towards the bays and sea is approximately equal for all four simulations. The outflow to the bays is 40-50% of the total outflow. While the outflow to the sea is 50-60% of the total outflow.

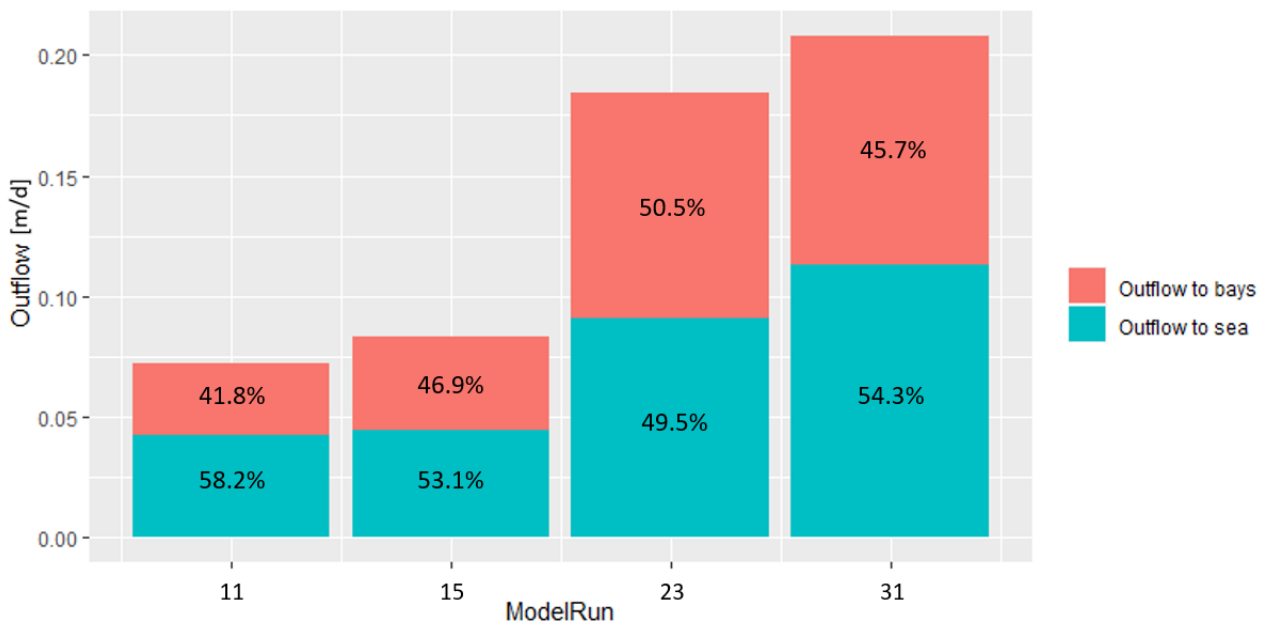


Figure 13: Outflow to sea and bays for four different model runs (11, 15, 23, 31) with the lowest Root Mean Square Error (R.M.S.E.).

## 4.2 Cross-sectional model

### 4.2.1 Cross-sectional area

The location of the cross-section depends on the flow lines of the regional plan view model described in Chapter 4.1.1 (Appendix E). The location is visualised in Figure 14. This cross-section has a length of 7.5 km, of which 7 km is through land and 500 m through the sea. The total outflow for the cross-section in the regional plan view model with the average input parameters is equal to 0.086 m/d. Based on the geological map, this cross-section crosses two geological formations. A small part of this are the limestone deposits around the coast. The largest part is the Curaçao Lava Formation which is present in the center of the island. This Limestone Formation consist of the Neogene Seroe Domi Formation and the Limestone Terraces. The Neogene Seroe Domi Formation unconformably overlies the Curaçao Lava Formation with a 350 m-thick deposition of seaward dipping (between 15 - 25°) dolomitised limestones (Figure 15). This formation is cropping out along the leeward coast of Curaçao. This Seroe Domi Formation can be subdivided in several subunits with different lithofacies. Near the coast, the limestone terraces are exposed. The seaward dipping limestones are incorporated in the cross-sectional model.

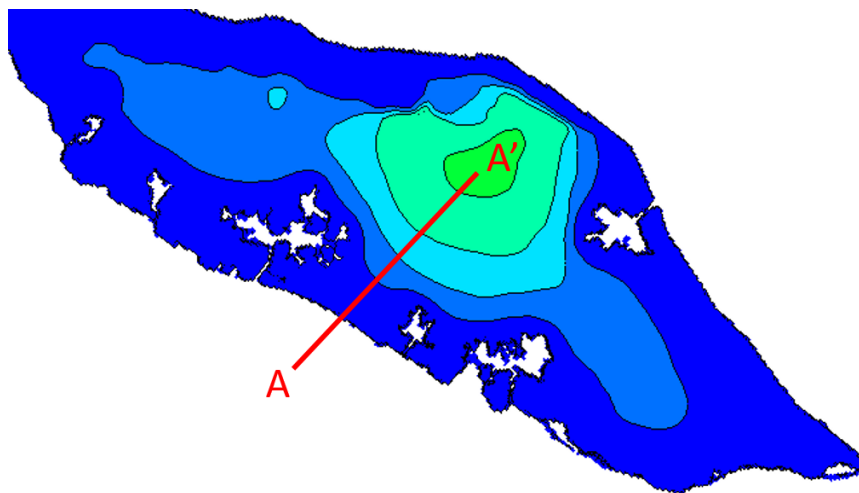


Figure 14: Location cross-section

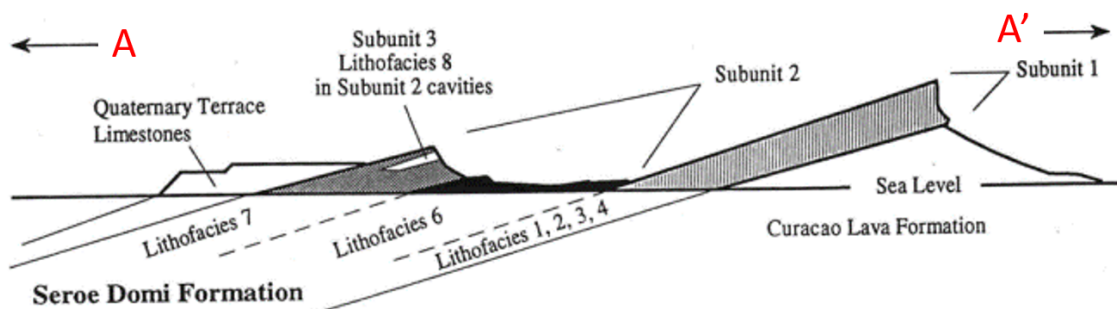


Figure 15: Seaward dipping Limestone Formation consisting of the Seroe Domi Formation with three different subunits and Quaternary limestone terraces. This Limestone Formation overlies the Curaçao Lava Formation (Fouke et al., 1996)

#### 4.2.2 Variable density groundwater flow

The entire model structure consists of a matrix of 1500 cells in the x-direction and 50 cells in the z-direction. The cells are composed of the same regular rectangles with a cell size of 5 x 5 m. The Curaçao Lava Formation and the Limestone Formation have different hydrogeological characteristics. The basalt and seaward dipping limestone are considered homogeneous within their layer. The properties of the Limestone Formation and Curaçao Lava Formation are described in Table 5. The layering of the geology (Chapter 4.2.1) is incorporated in the model. This is done by including the hydraulic conductivity, specific yield, specific storage and porosity of the Limestone Formation and Curaçao Lava Formation at the corresponding cells. On the top layer a constant recharge is applied with a uniform flux of  $7.86E-05$  m/d (Chapter 3.1.2) and concentration of  $1.8 \text{ kg m}^{-3}$ . This salt recharge concentration is obtained from the electrical conductivity (EC) depth profile that is located in the cross-section (Chapter 2.2.3). In Figure 16, the conceptual model of the cross-section is shown. The seaward dipping limestones are incorporated in the simulation.

Table 5: Input parameter for the Curaçao Lava Formation (Basalt) and the Limestone Formation.

Formation	Parameter	Value	Units	Source
<b>Basalt</b>	Hydraulic conductivity	6.1	[m/d]	(Abtmaier, 1978)
	Specific storage	3.60E-05	[m <sup>-1</sup> ]	(Batu, 1998)
	Specific yield	1.5	[%]	(Abtmaier, 1978)
	Porosity	17	[%]	(Batu, 1998)
<b>Limestone</b>	Hydraulic conductivity	15	[m/d]	(Domenico et al., 1998; Whitaker, Smart, 1997)
	Specific storage	3.60E-05	[m <sup>-1</sup> ]	(Batu, 1998)
	Specific yield	18	[%]	(Heath, 1998)
	Porosity	3	[%]	(Batu, 1998)

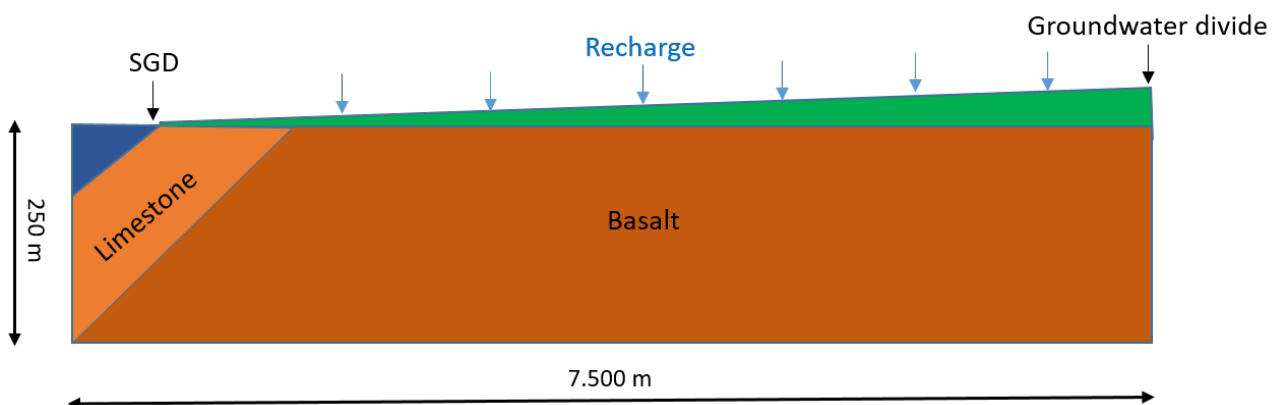


Figure 16: Conceptual model of 2D cross-section. The cross-section is vertical exaggerated. Therefore, seaward dipping limestone visualised in the figure consists of an angle of  $\geq 15 - 25^\circ$ .

The development of the freshwater lens is visualised in Figure 17. The run time of the model was 2500 years. At this time step the freshwater/saltwater interface hardly changed. Stable conditions are reached after 2500 years. At this time step, the thickness of the freshwater lens is increased to

145 m. The transition zone between freshwater and saltwater has a thickness of approximately 15 m. The dominant groundwater flow is towards the sea. Around this location, the fresh groundwater leaves the aquifer. This is due to the fact that there is an outflow of water over the boundary condition. The freshwater/saltwater interface is only slightly influenced by the seaward dipping limestone formations. The freshwater lens grows slightly when it reaches the basaltic rocks (right of the black line in Figure 17).

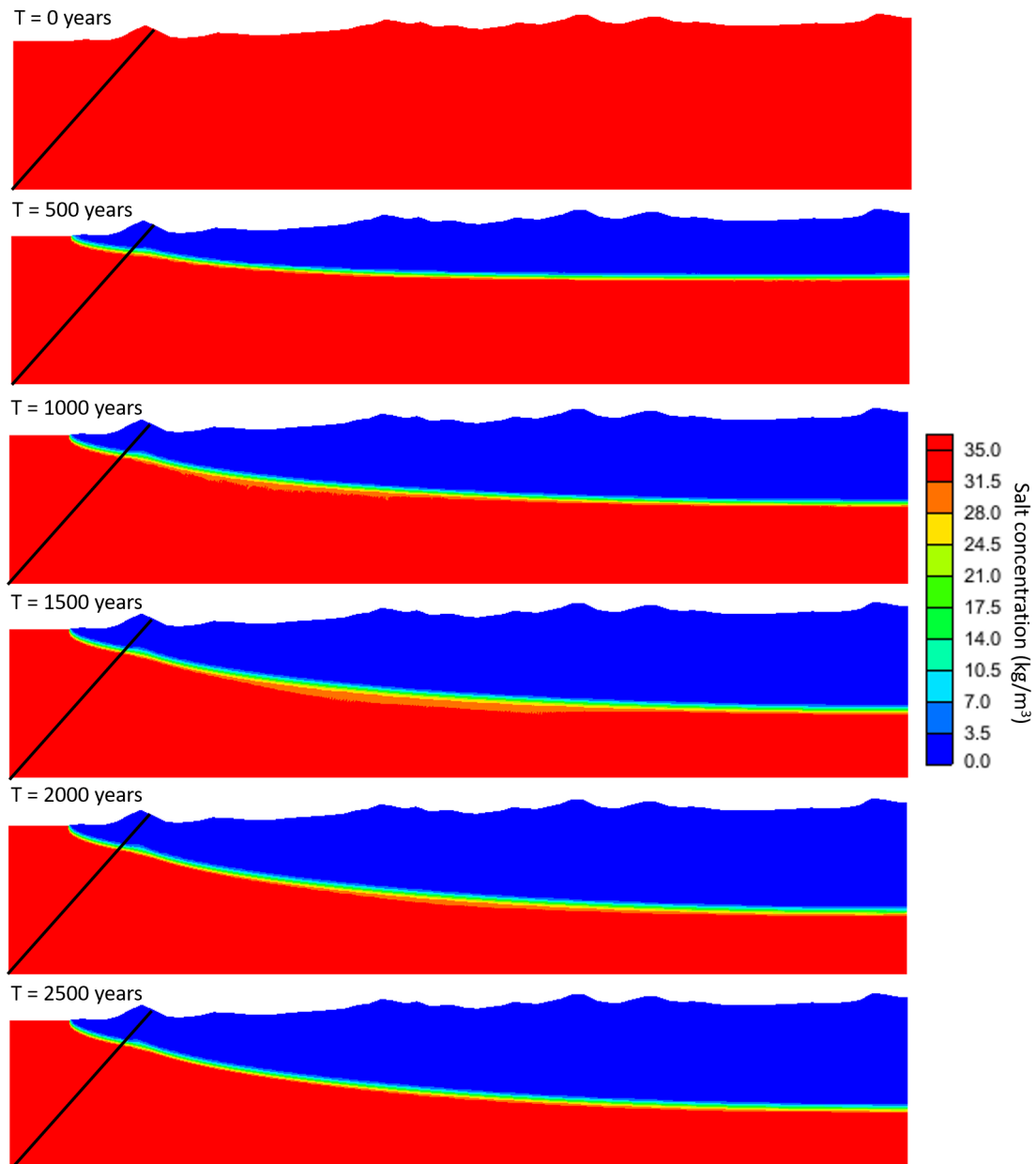


Figure 17: Development of freshwater lens for time steps of 500 years. Stable freshwater lens in 2500 years. The black line on the left side of the cross-section shows the transition between limestone and basaltic rocks.

The freshwater/saltwater interface also affects the hydraulic heads in the cross-section. Figure 18 shows the development of the hydraulic heads in the cross-section. The maximal hydraulic head is 3.61 m on the right side of the cross-section. Below the freshwater/saltwater interface the values for the hydraulic head are negative.

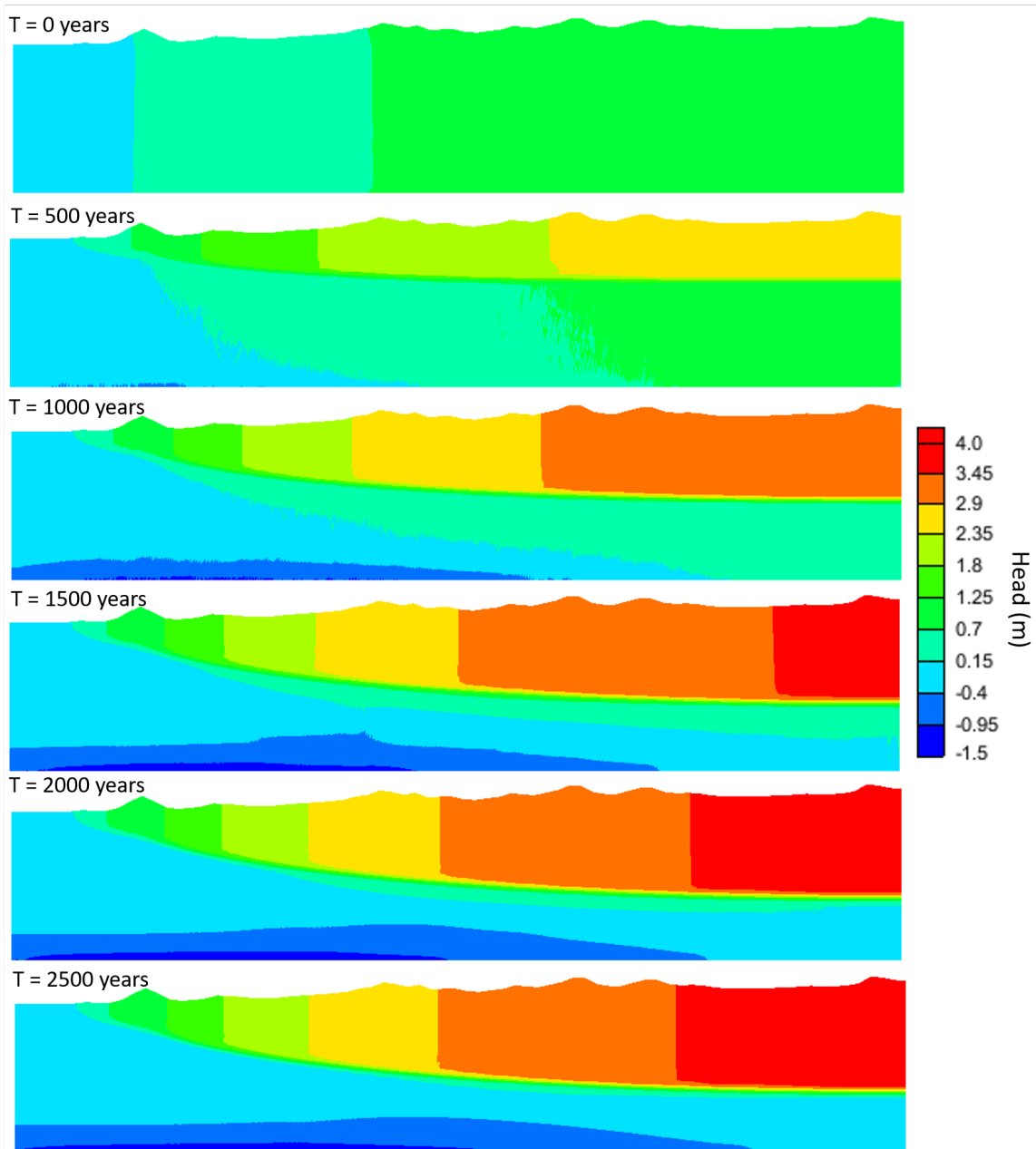


Figure 18: Hydraulic head development over time with time steps of 500 years.

### 4.2.3 Submarine groundwater discharge

The SGD is determined by the outflow over the boundary. For this cross-section, the zoomed-in situation around the boundary condition is visualised in Figure 18. The velocity vectors are pointing horizontally, until they reach the freshwater/saltwater interface. At this point, the velocity vectors are following the interface and the magnitude of the vectors increases. The velocity vector with the largest magnitude (red arrow) is located at the first cell where a boundary conditions applies seen from the land. The outflow is occurring for the cells that are appointed as specified heads. Only the first specified head cell, seen from the land, generates outflow in the sea. The amount of outflow is equal to 0.15 m/d. This amount is depending on the amount of recharge, due to the fact that this is the only source of inflow. For the other cells that function as boundary condition no outflow is observed.

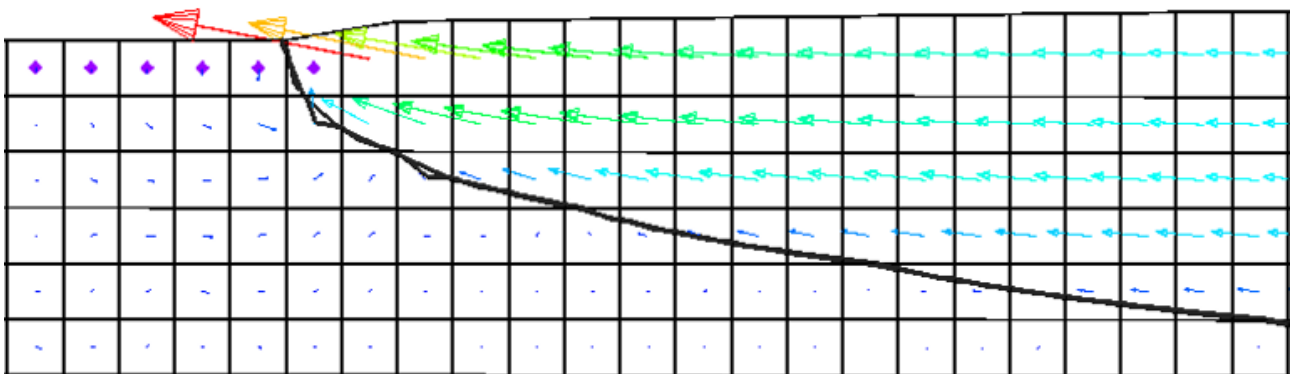


Figure 19: Outflow of groundwater over the boundary condition. The velocity vectors are indicated with the colored arrows, where red means high velocity and blue means low velocity. The thick black line is the the freshwater/saltwater interface and the boundary condition is shown as purple diamonds.

## 5 Discussion

In this chapter the use of the groundwater models is discussed. The first subsection considers the effect of the input parameters on the regional plan view model. Moreover, the comparison with observation is discussed in this subsection. The next subsection explains the choice for the cross-sectional model and the consequences of this choice. In this third subsection the quantification of the SGD is discussed. The last subsection contains recommendations for further research.

### 5.1 Regional plan view model

With the regional plan view model the groundwater flow on Curaçao was modelled. Density effect were neglected for this model. Therefore, the assumption was that the groundwater only consists of freshwater. The simulated groundwater levels were affected by the geological formations. By averaging the outcomes of the pumping tests, the hydraulic conductivity receives one specific value per geological formation. The groundwater levels increased for formations with a lower hydraulic conductivity (Mid Curaçao Formation). The opposite occurred for a formation with a high hydraulic conductivity (Limestone Formation). In the northern and southern part of Curaçao two groundwater bulges were simulated. This results in a groundwater flow towards the coast. The thickness of the aquifer was depending on the depth of the groundwater wells drilled for the study of Abtmaier (1978). However, around the coast this thickness is influenced by the density differences due to the interaction with seawater. These density effects on the groundwater flow were evaluated in the cross-sectional model.

This predominant flow direction is affected by the heterogeneity of the geological formation itself. Volcanic and karstic rocks contain a considerable spatial heterogeneity on a small scale (Ghasemizadeh et al., 2012; Taniguchi et al., 2019). The regional plan view model with a cell size of 100 x 100 m is unable to represent this heterogeneity. The model was not able to simulate the groundwater flow affected by cracks and conduit flows. Higher outflow fluxes can be perceived at locations where conduits flow are present and linked to the sea or bays. Therefore, the outflow towards the bays and sea for the entire coast is spatially variable. However, the average SGD for the entire island ignores this spatial variability. The total outflow for the four model runs with the lowest R.M.S.E. (Chapter 4.1.3) ranges from 0.07-0.21 m/d, which is equal to 25.6-76.7 m/year. Taniguchi et al. (2002) described the calculated SGD for 45 locations on earth. The SGD ranged from 0.03-454 m/year for aquifers in different geological formations and climatic conditions. According to Taniguchi et al. (2002), the SGD is highly variable for different locations with different geology and climate. Therefore, the SGD on Curaçao will be spatially and temporally variable. Moreover, the total outflow on Curaçao is highly affected by the bays. About half of the groundwater flows towards these bays. Therefore, the SGD on Curaçao will be spatially and temporally variable. To understand and quantify this spatial and temporal variability new methods need to be used. To quantify SGD in karstic or fractured bedrock environments, a combination of methods to determine the SGD is preferred (Burnett et al., 2006).

As described in Chapter 4.1.2, the groundwater model is highly affected by the input parameters.  $K_{CLF}$  and  $K_{Limestone}$  are the most influential on the groundwater distribution. The effect of  $K_{Mid}$  and  $K_{Knip}$  is limited to local differences. The magnitude of the groundwater levels is determined by the recharge flux and the hydraulic conductivity. These input parameters are highly correlated. A high recharge flux in combination with a low hydraulic conductivity resulted in a overestimation of the groundwater levels, due to a larger Root Mean Square Error (R.M.S.E.). Surface runoff should be

included for simulations with too high groundwater levels. Due to a low hydraulic conductivity and high recharge flux, the inflow is larger than the outflow. As a result, the infiltration capacity would be too small and surface runoff would occur. However, for the average parameter simulation and the four best model runs from the parameter analysis performed in this study, surface runoff was negligible. The geological formation with the largest influence on the uncertainty of the model was the hydraulic conductivity of the Curaçao Lava Formation. Lower values lead frequently to a larger R.M.S.E. This can be explained by the fact that the Curaçao Lava Formation is the most abundant geological formation on Curaçao. Therefore, the influence of the parameter on the the uncertainty of the model is larger compared to the other geological formations. Furthermore, higher recharge values lead more often to a larger R.M.S.E. The optimal range of recharge values is between 0.00004 and 0.0002 m/d, which is equal to 14.6-73 mm/year. The average recharge appointed by De Vries (2000) lies within this range. The average recharge according to De Vries (2000) is 5% of the precipitation, which is equal to 28.7 mm/year.

The parameter analysis was not performed for the independent input parameters, solely the effect of the main input parameters (hydraulic conductivity and recharge) on the outflow was studied. This was examined by calculating the R.M.S.E. by comparing the modelled hydraulic heads with the observed hydraulic heads. However, calibration of the groundwater model was not possible, due to insufficient field data. In addition, the groundwater levels measurements were conducted for a specific moment in time. These groundwater levels are affected by the recent weather influences. The groundwater level measurements were conducted in the rainy season. Therefore, the observed hydraulic heads were to some extent overestimated. The yearly average of the groundwater levels could not be used, because no data were available for the yearly variability of the groundwater levels. The local variability of the hydrogeological properties generate a complex model evaluation. Especially in geological formations with karstic or volcanic origin the calibration of the regional plan view model was unfeasible with limited field data. Nevertheless, the comparison with the observations was useful, because the evaluation of the errors led to a better understanding of the groundwater flow patterns.

## 5.2 Cross-sectional model

For this cross-sectional groundwater model the effect of density dependent flow was incorporated. The freshwater aquifers on Curaçao are influenced by the marine environment. The interaction between freshwater and saltwater is important for the simulation of groundwater. For this model it was chosen to use a 2D cross-section. Due to insufficient field data and high computational demand it was unfeasible to incorporate the density dependent flow in the regional plan view model. Therefore, the cross-sectional model was constructed and a specific cross-section on Curaçao was selected. For this 2D cross-section, the flow was assumed to be perpendicular to the flow lines of the regional plan view model. Therefore, no inflow from other directions was expected for this model. The volcanic and karstic formations contain preferential flow paths, which can cause flow in other directions. This inflow and outflow of the cross-section from the water divide to the coast was assumed to be equal. Because of that simplification, it was possible to simulate the groundwater flow in this 2D cross-section.

The freshwater lens reaches a thickness of 145 m. This is in agreement with the Ghyben-Herzberg ratio (Essaid, 1986). This ratio states that the freshwater head multiplied with 40 (ratio between freshwater ( $\rho_f$ ) and saltwater ( $\rho_s$ )) gives the freshwater lens. The maximum calculated freshwater



head for the 2D cross-section is 3.61 m. Therefore, the maximum freshwater head according to the Ghyben-Herzberg ratio is  $3.61 * 40 = 144$  m. The interface is only slightly influenced by the seaward dipping limestone formations. This seaward dipping limestone formation contains a larger hydraulic conductivity compared to the Curaçao Lava Formation. Therefore, seaward intrusion is more likely to occur at this location (Costall et al., 2020). Saltwater migrates laterally inland and shifts the freshwater/saltwater interface slightly in the same direction.

The density dependent groundwater flow resulted in an outflow over the boundary of 0.15 m/d. This outflow lies within the range of the regional plan view model (0.07-0.21 m/d). This outflow is discharged at one specific cell in the cross-section. In general, the outflow will be spatially variable around the transition zone between the aquifer and the seawater. The outflow will occur at locations where the groundwater leaves the aquifer and reaches the marine environment. The location of the conduits and the preferential flow paths are unknown. At these locations higher outflows will be expected.

The regional plan view model and cross-sectional model are compared based on the hydraulic heads simulated for both models. The maximum hydraulic head for the cross-section in the regional plan view model is 5.0 m. The maximum hydraulic head for the simulation with density effects included is 3.61 m. Therefore, the regional plan view model generates higher groundwater levels compared to the cross-sectional model. On the other hand, the total outflow of the cross-section in the regional plan view is smaller. The SGD for this model is equal to 0.086 m/d compared to 0.15 m/d for the cross-sectional model. Due to the smaller outflow, the maximum hydraulic head is larger for regional plan view model where density effects are neglected. Therefore, the groundwater levels in the regional plan view model are slightly overestimated. On the other hand, the total outflow is slightly underestimated.

### 5.3 Submarine groundwater discharge

The purpose of this study was not to simulate the temporal and spatial variability of SGD in Curaçao in a high degree of accuracy. The complexity of the geological formation with karstic and volcanic formations limits the ability to do this with confidence. Temporal processes such as recirculation of seawater, wave action, extreme precipitation and groundwater abstractions influence the SGD as well (Costall et al., 2020). The goal of this study was to assess the groundwater flow patterns and to quantify the average SGD. Other studies also quantified this SGD for islands with karstic formations. Table 6 lists three studies reporting the quantification of SGD for islands with karst formations. In general, the SGD increases with increasing precipitation (Zhang et al., 2017).

Table 6: Identified studies quantifying SGD from islands with karst formations and the relation with annual precipitation.

<b>Location</b>	<b>SGD</b> <i>m/year</i>	<b>SGD</b> <i>m/d</i>	<b>Precipitation</b> <i>mm/year</i>	<b>Source</b>
Barbados	361	0.99	1350	(Lewis, 1987)
Heron Island, Australia	55	0.15	1027	(Santos et al., 2010)
Majorca, Spain	38	0.10	410	(Basterretxea et al., 2010)
Curaçao	55	0.15	574	This study

The simplifications and/or assumptions made in the model have an impact on the results. Because of this, it was complex to capture the spatial and temporal variability of the SGD. However, it was possible to approximate the average SGD with this numerical modelling study. The average SGD on Curaçao is of the same order of magnitude as the average SGD for Majorca and Heron Island. Although the spatial and temporal variability must be kept in mind, because the amount of SGD is not a fixed amount. The flux of groundwater, which can transport nutrients and contaminants, has an impact on the health of the coral reefs around Curaçao. A study conducted by (Lubarsky et al., 2018) in Hawaii indicates the effect of SGD on the coral growth. This study showed that a moderate enrichment by SGD allows for an increase in coral growth. However, a larger SGD flux induces mortality of the coral reef. Because of that, the coral growth decreases. The effect of SGD on coral growth in Curaçao therefore depends on the nutrient and pollutant concentrations in the groundwater and the concentration that ends up in the marine environment. This needs to be evaluated in future research.

## 5.4 Recommendations

With the experiences obtained in this research, several recommendations can be made regarding the quantification of SGD:

- A combination of multiple methods will result in more accurate approximation of the SGD. Possible measurement techniques to assess SGD are geochemical tracers, seepage meters, multi-level piezometer nests and a water balance approach (Burnett et al., 2006). These methods all have their advantages and disadvantages. Therefore, it is recommended to use a variety of methods to capture both spatial and temporal scales.
- For the groundwater models it is important to analyse the recharge to the aquifers. This recharge flux is spatially and temporally variable (Hartmann et al., 2012). Precipitation, geology and land use are the main drivers of this flux. Therefore, additional field measurements are necessary to determine the variability of the recharge flux to the aquifers on Curaçao.
- Further research should be obtained about the hydrogeological properties of the geological formations. Especially additional information about the heterogeneity and anisotropy of Limestone Formation is necessary, because this formation is mainly exposed adjacent to the sea and can contain preferential flow paths. Therefore, the groundwater flux towards the marine environment is highly affected by this geological formation. Additional measurements may include more pumping tests to determine the type of pumping test response. Moreover, core analysis, packer tests and specific capacity tests examine the range of the hydraulic conductivity values and the presence of fracture or double-porosity flow systems.

## 6 Conclusion

The groundwater patterns in Curaçao are affected by the geological formations. The hydraulic conductivity between the geological formations is variable. From low values for the Mid Curaçao Formation, to high values for the Limestone Formation. The regional plan view model simulates two large groundwater bulges in the southern and northern part of the island. The groundwater is transported from these groundwater bulges towards the sea or one of the many bays. The combination of relatively narrow cells and a low hydraulic conductivity results in the highest groundwater levels. This can be observed for the area where the Mid Curaçao Formation is present.

The regional plan view is highly affected by the input parameters. The distribution of the groundwater levels is mainly depending on the  $K_{CLF}$  and  $K_{Limestone}$ . The effect of  $K_{Mid}$  and  $K_{Knip}$  is limited to local differences. The magnitude of the groundwater levels is determined by the recharge flux and the hydraulic conductivity. In general, model runs with a relatively large recharge flux ( $\geq 0.0002$  m/d) create a large uncertainty in the model output, because the simulated heads deviate substantially from the observed heads. The optimal range of recharge values is between 0.00004 and 0.0002 m/d, which is equal to 14.6 - 73 mm/year. The other input parameter that has a large impact on the model output is the hydraulic conductivity. The Curaçao Lava Formation is the most abundant geological formation on Curaçao. Therefore, the hydraulic conductivity of this formation has the largest influence on the uncertainty of the model. Lower values ( $\leq 0.4$  m/d) lead frequently to a larger Root Mean Square Error (R.M.S.E.).

The density dependent groundwater flow was incorporated in the cross-sectional model. The freshwater lens reaches a thickness of 145 m, with a transition zone between freshwater and saltwater of approximately 15 m. The interface is only slightly influenced by the seaward dipping limestone formations. This seaward dipping limestone formation contains a larger hydraulic conductivity compared to the Curaçao Lava Formation. Therefore, seaward intrusion is more likely to occur at this location. Saltwater migrates laterally inland and shifts the freshwater/saltwater interface slightly in the same direction.

The influence of the geological formations, model parameters and density dependent flow provide an approximation of the SGD on Curaçao. The total outflow for the entire island was generated with the parameter analysis of the regional plan view model. The four model runs with the lowest error simulated an outflow of 0.07 - 0.21 m/d. About half of this flows into the bays, and the other half is discharged as SGD. The freshwater/saltwater interface has a considerable effect on the outflow over the boundary. The outflow for the simulation of cross-section with only freshwater resulted in an outflow of 0.086 m/d, compared to 0.15 m/d for the density dependent flow simulation. Due to the smaller outflow, the maximum hydraulic head is larger for regional plan view model where density effects are neglected. Therefore, the groundwater levels in the regional plan view model are slightly overestimated. On the other hand, the total outflow is slightly underestimated. The amount of total outflow is comparable with other studies that quantified the SGD for karstic islands, although a combination of methods is preferred to capture the spatial and temporal variability of the SGD.

## **Acknowledgments**

First of all, I would like to thank my supervisors George Bier and Victor Bense for their help during my thesis. The interesting meetings and the constructive feedback have helped me a lot during this period. Moreover, I want to thank Titus Kruijssen for providing and discussing field data obtained in Curaçao. Furthermore, I would like to thank the SEALINK project and everyone linked to it for sharing data of field measurements. I also want to thank CARMABI for providing the Digital Elevation Model. Lastly, I want to thank my fellow students for useful feedback and pleasant discussions.

## Bibliography

- Abtmaier B.F.* Groundwater investigation - Curacao. 1978.
- Aghlmand R., Abbasi A.* Application of MODFLOW with boundary conditions analyses based on limited available observations: A case study of Birjand plain in East Iran // *Water*. 2019. 11, 9. 1904.
- Bakalowicz M.* Karst groundwater: a challenge for new resources // *Hydrogeology Journal*. feb 2005. 13, 1. 148–160.
- Basterretxea G., Tovar-Sanchez A., Beck A.J., Masqué H.J. P. and Bokuniewicz, Coffey R., Duarte C. M., Garcia-Orellana J., Garcia-Solsona E., Martinez-Ribes L. and others.* Submarine groundwater discharge to the coastal environment of a Mediterranean island (Majorca, Spain): ecosystem and biogeochemical significance // *Ecosystems*. 2010. 13, 5. 629–643.
- Batu V.* Aquifer hydraulics: a comprehensive guide to hydrogeologic data analysis. 1998.
- Beets D., MacGillavry H.* Guide to the field excursions on Curacao, Bonaire and Aruba, Netherlands antilles. 1977. (1).
- Beets D.J.* Geologic Map of Curacao 1:50000. 1972.
- Burnett W.C., Aggarwal P.K., Aureli A., Bokuniewicz H., Cable J.E., Charette M.A., Kontar E., Krupa S., Kulkarni K.M., Loveless A., others.* Quantifying submarine groundwater discharge in the coastal zone via multiple methods // *Science of the total Environment*. 2006. 367, 2-3. 498–543.
- Costall A.R., Harris B.D., Teo B., Schaa R., Wagner F.M., Pigois J.P.* Groundwater throughflow and seawater intrusion in high quality coastal aquifers // *Scientific reports*. 2020. 10, 1. 1–33.
- De Vries A.J.* The semi-arid environment of Curaçao: a geochemical soil survey // *Netherlands Journal of Geosciences - Geologie en Mijnbouw*. dec 2000. 79, 4. 479–494.
- Debrot A., Wells J.* s CURAÇAO. 2008.
- Den Haan J., Huisman J., Brocke H.J., Goehlich H., Latijnhouwers K.R.W., Van Heeringen S., Honcoop S.A.S., Bleyenbergh T.E., Schouten S., Cerli C., others.* Nitrogen and phosphorus uptake rates of different species from a coral reef community after a nutrient pulse // *Scientific reports*. 2016. 6, 1. 1–13.
- Domenico P.A., Schwartz F.W., others.* Physical and chemical hydrogeology. 506. 1998.
- El Mezouary L., El Mansouri B.* Applied Latin Hypercube stochastic method to quantify the uncertainty in groundwater equation model simulations // *E3S Web of Conferences*. 314. 2021. 04008.
- Essaid H.I.* A comparison of the coupled fresh water-salt water flow and the Ghyben-Herzberg sharp interface approaches to modeling of transient behavior in coastal aquifer systems // *Journal of Hydrology*. 1986. 86, 1-2. 169–193.
- Estep A., Sandin S., Vermeij M.* The state of curacao's coral reefs. The Waitt Institute. 2017.

- Fouke B.W., Beets C.J., Meyers W.J., Hanson G.N., Melillo A.J.*  $^{87}\text{Sr}/^{86}\text{Sr}$  chronostratigraphy and dolomitization history of the Seroe Domi Formation, Curacao (Netherlands Antilles) // *Facies*. 1996. 35, 1. 293–320.
- Ghasemizadeh R., Hellweger F., Butscher C., Padilla I., Vesper D., Field M., Alshawabkeh A.* Groundwater flow and transport modeling of karst aquifers, with particular reference to the North Coast Limestone aquifer system of Puerto Rico // *Hydrogeology journal*. 2012. 20, 8. 1441–1461.
- Global Coral Reef Monitoring Network* . Status and Trends of Caribbean Coral Reefs: 1970-2012. 2014.
- Guo W., Langevin C.D.* User's guide to SEAWAT; a computer program for simulation of three-dimensional variable-density ground-water flow. 2002.
- Hartmann A., Lange J., Weiler M., Arbel Y., Greenbaum N.* A new approach to model the spatial and temporal variability of recharge to karst aquifers // *Hydrology and Earth System Sciences*. 2012. 16, 7. 2219–2231.
- Heath R.C.* Basic ground-water hydrology. 2220. 1998.
- Hugman R.* Numerical approaches to simulate groundwater flow and transport in coastal aquifers—from regional scale management to submarine groundwater discharge. 2017.
- Kaleris V., Lagas G., Marczynek S., Piotrowski J.A.* Modelling submarine groundwater discharge: an example from the western Baltic Sea // *Journal of Hydrology*. 2002. 265, 1-4. 76–99.
- Konikow L.F., Reilly T.E., Barlow P.M., Voss C.I.* The Handbook of Groundwater Engineering. nov 2006.
- Langevin C.D., Hughes J.D., Banta E.R., Niswonger R.G., Panday S., Provost A.M.* Documentation for the MODFLOW 6 groundwater flow model. 2017.
- Lewis J.B.* Measurements of groundwater seepage flux onto a coral reef: Spatial and temporal variations // *Limnology and Oceanography*. 1987. 32, 5. 1165–1169.
- Liu G., Zhang D, Lu Z.* MODFLOW-STO: Stochastic Modeling of Flow in Saturated Porous Media Using MODFLOW-2000 // AGU Fall Meeting Abstracts. 2005. 2005. H23F–1495.
- Louws R.J., Vriend S.P., Frapporti G.* De grondwaterkwaliteit van Curacao // *H2O*. 1997. 30, 26.
- Lubarsky K.A., Silbiger N.J., Donahue M.J.* Effects of submarine groundwater discharge on coral accretion and bioerosion on two shallow reef flats // *Limnology and Oceanography*. 2018. 63, 4. 1660–1676.
- Luoma S., Majaniemi J., Pullinen A., Mursu J., Virtasalo J.J.* Geological and groundwater flow model of a submarine groundwater discharge site at Hanko (Finland), northern Baltic Sea // *Hydrogeology Journal*. 2021. 29, 3. 1279–1297.
- McDonald M.G., Harbaugh A.W.* A modular three-dimensional finite-difference ground-water flow model. 1988.
- Moberg F., Rönnbäck P.* Ecosystem services of the tropical seascape: interactions, substitutions and restoration // *Ocean & Coastal Management*. 2003. 46, 1-2. 27–46.

- Moore W.S.* The Effect of Submarine Groundwater Discharge on the Ocean // *Annual Review of Marine Science*. jan 2010. 2, 1. 59–88.
- Moosdorf N., Stieglitz T., Waska H., Dürr H., Hartmann J.* Submarine groundwater discharge from tropical islands: a review // *Grundwasser*. dec 2014. 20, 1. 53–67.
- Mugunthan P., Shoemaker C.A.* Assessing the impacts of parameter uncertainty for computationally expensive groundwater models // *Water Resources Research*. 2006. 42, 10.
- Oberdorfer J.A.* Hydrogeologic modeling of submarine groundwater discharge: comparison to other quantitative methods // *Biogeochemistry*. 2003. 66, 1. 159–169.
- Pandolfi J.M.* The paleoecology of coral reefs // *Coral reefs: an ecosystem in transition*. 2011. 13–24.
- Prieto C.* Groundwater-seawater interactions: Seawater intrusion, submarine groundwater discharge and temporal variability and randomness effects. 2005.
- Santos I.R., Chen X., Lecher A.L., Sawyer A.H., Moosdorf N., Rodellas V., Tamborski J., Cho H., Dimova N., Sugimoto R., Bonaglia S., Li H., Hajati M., Li Ling.* Submarine groundwater discharge impacts on coastal nutrient biogeochemistry // *Nature Reviews Earth & Environment*. mar 2021. 2, 5. 307–323.
- Santos I.R., Erler D., Tait D., Eyre B.D.* Breathing of a coral cay: Tracing tidally driven seawater recirculation in permeable coral reef sediments // *Journal of Geophysical Research: Oceans*. 2010. 115, C12.
- Senger R.K., Fogg G.E.* Stream functions and equivalent freshwater heads for modeling regional flow of variable-density groundwater: 1. Review of theory and verification // *Water Resources Research*. 1990. 26, 9. 2089–2096.
- Street J.H., Knee K.L., Grossman E.E., Paytan A.* Submarine groundwater discharge and nutrient addition to the coastal zone and coral reefs of leeward Hawai'i // *Marine Chemistry*. apr 2008. 109, 3-4. 355–376.
- Taniguchi M., Burnett W.C., Cable J.E., Turner J.V.* Investigation of submarine groundwater discharge // *Hydrological Processes*. 2002. 16, 11. 2115–2129.
- Taniguchi M., Dulai H., Burnett K.M., Santos I.R., Sugimoto R., Stieglitz T., Kim G., Moosdorf N., Burnett W.C.* Submarine groundwater discharge: updates on its measurement techniques, geophysical drivers, magnitudes, and effects // *Frontiers in Environmental science*. 2019. 7. 141.
- Van Sambeek M.H.G., Eggenkamp H.G.M., Vissers M.J.M.* The groundwater quality of Aruba, Bonaire and Curaçao: a hydrogeochemical study // *Netherlands Journal of Geosciences - Geologie en Mijnbouw*. dec 2000. 79, 4. 459–466.
- Vermeij M.* Caribbean research: a multidisciplinary approach. 2019.
- Werger M.J.A., Bok C. de, Oranje B.* Vegetation structure, phytomass and phenology of the dry thorn scrub of Curacao, West Indies // *Modern Ecology: Basic and Applied Aspects*. 2016. 21.
- Whitaker F.F., Smart P.L.* Climatic control of hydraulic conductivity of Bahamian limestones // *Groundwater*. 1997. 35, 5. 859–868.

---

*Zhang B., Zhang J., Yoshida T.* Temporal variations of groundwater tables and implications for submarine groundwater discharge: a 3-decade case study in central Japan // *Hydrology and Earth System Sciences*. 2017. 21, 7. 3417–3425.

*Zheng C., Wang P.P., others* . MT3DMS: a modular three-dimensional multispecies transport model for simulation of advection, dispersion, and chemical reactions of contaminants in groundwater systems; documentation and user's guide. 1999.



## Appendices

### A Groundwater level measurement locations

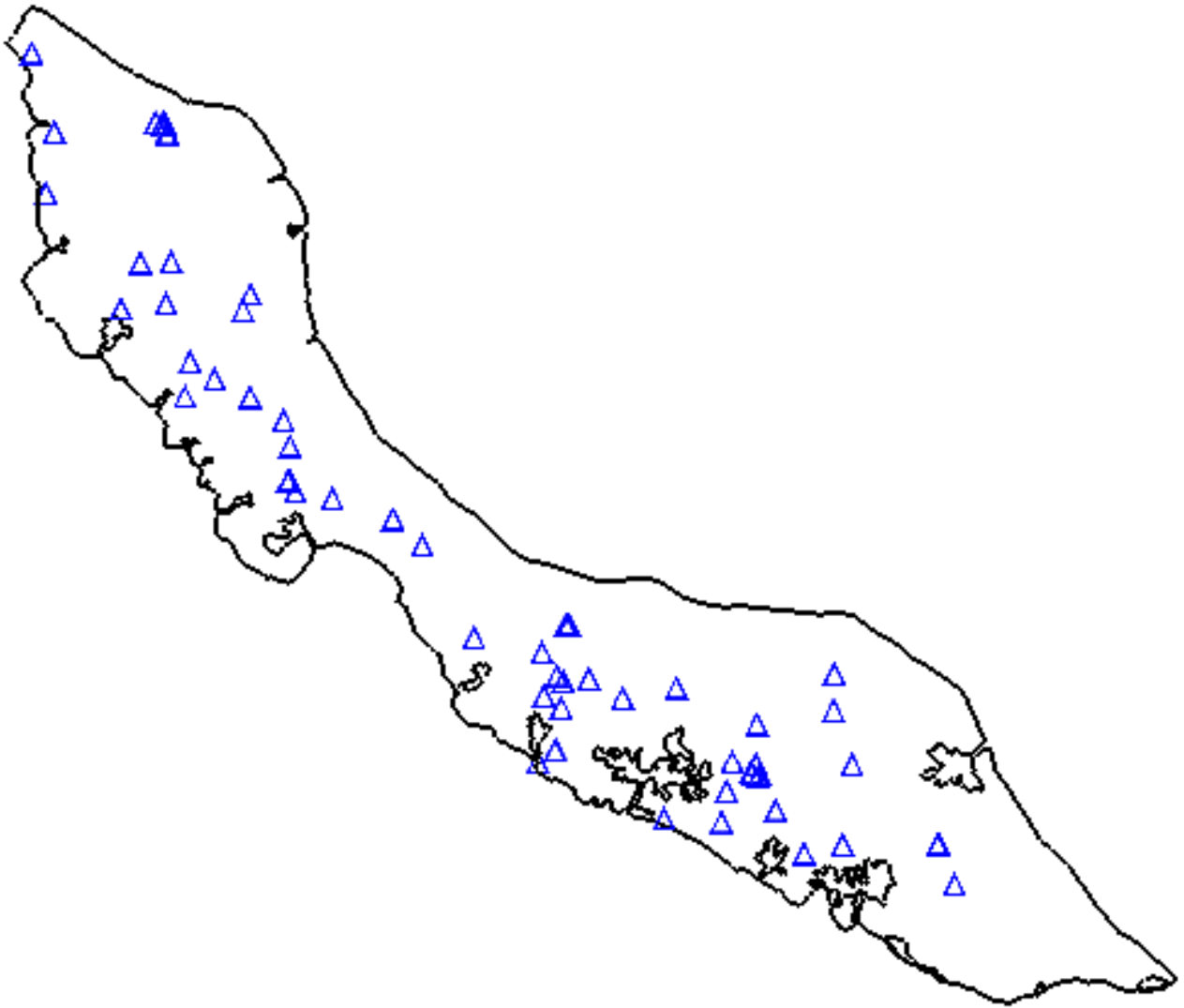


Figure 20: Location of measured groundwater wells

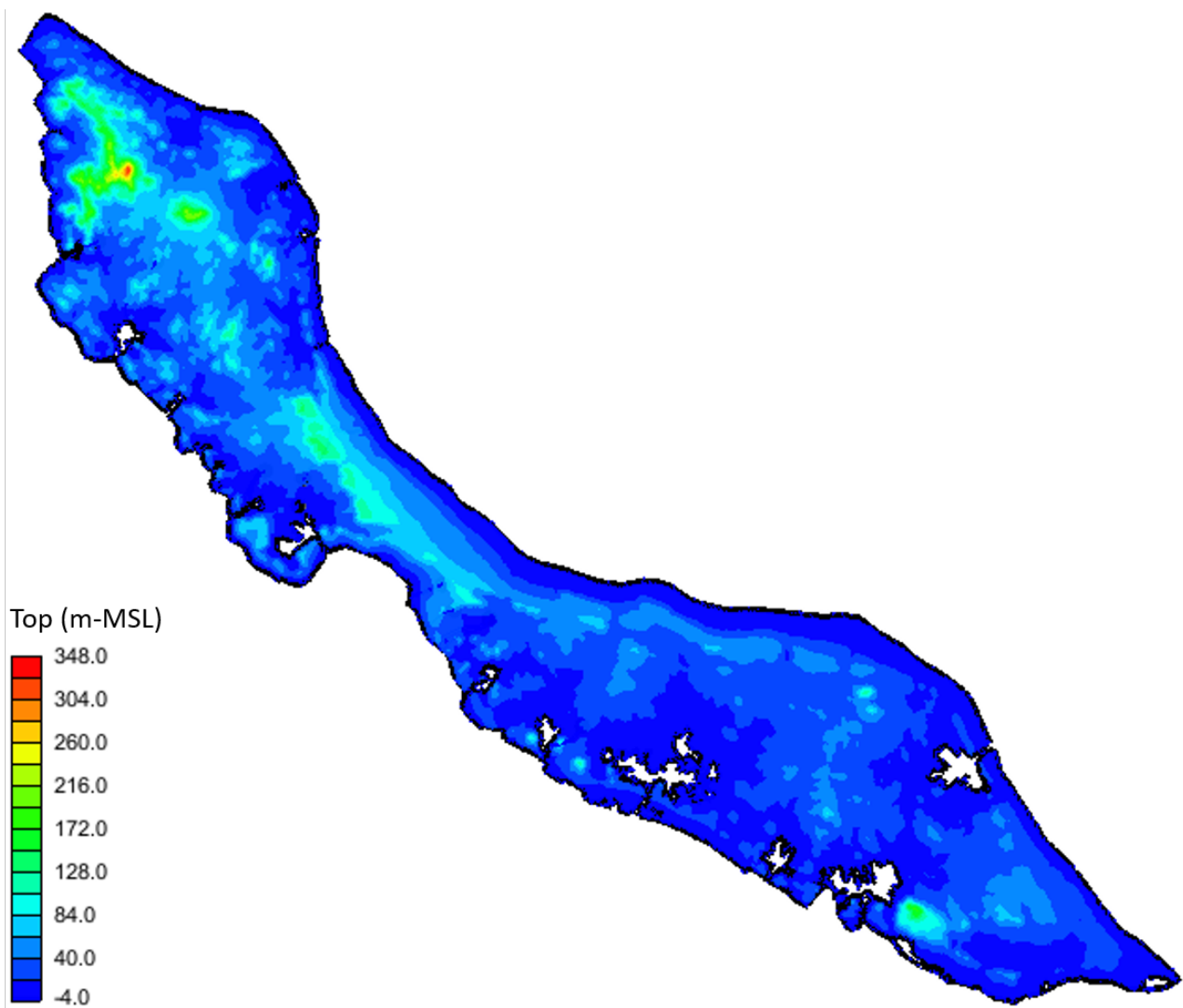
**B Top of the regional plan view model**

Figure 21: Top elevation based on Digital Elevation Model (DEM)

### C Bottom of the regional plan view model

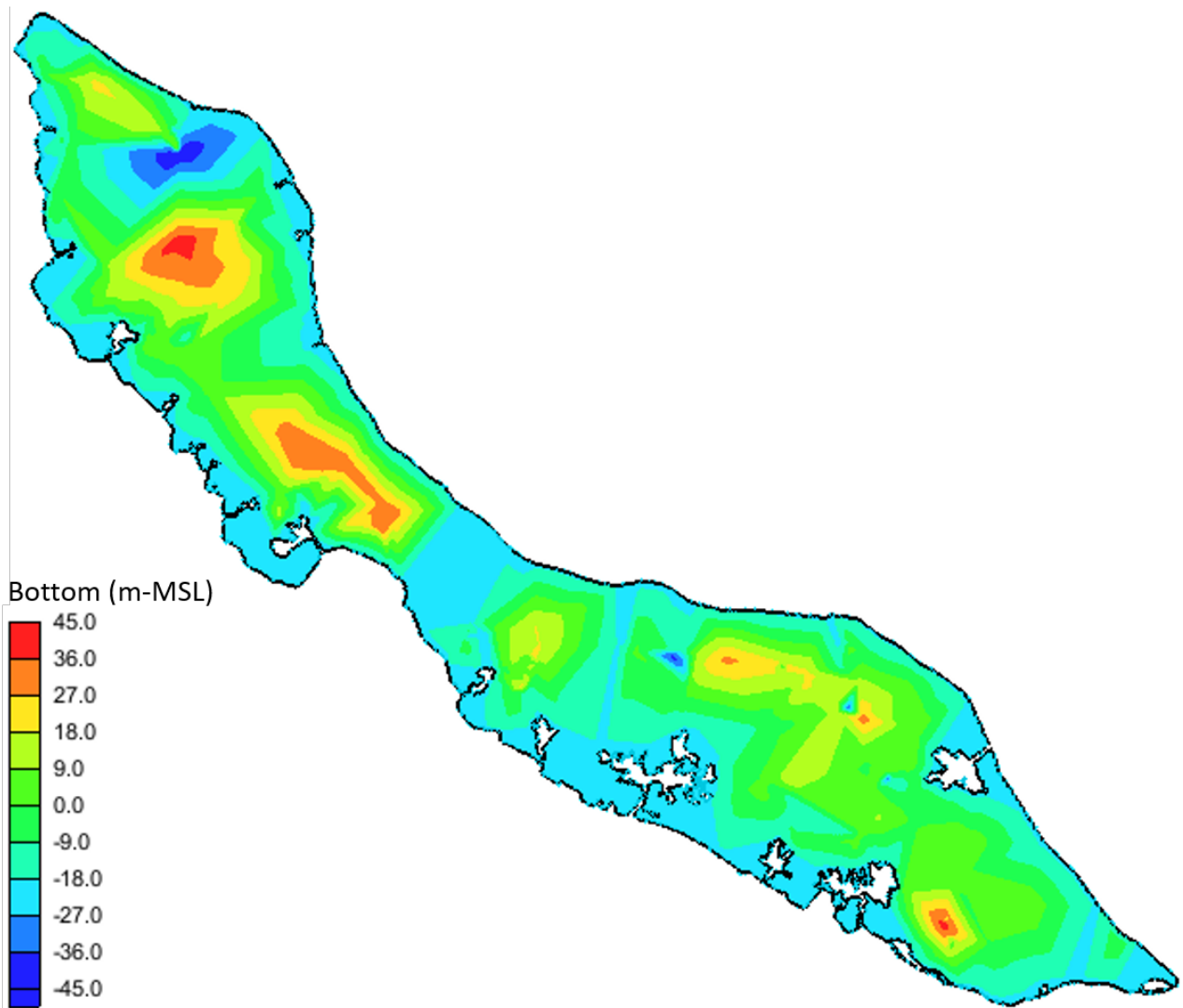


Figure 22: Bottom of the regional plan view model based on linear interpolation of the depth of the groundwater wells

## **D Parameter analysis**

Table 7: Input parameters and comparison with observations of all model runs. The minimum, maximum and average values are shown below. Highest 20% of the different input parameters is shown in red values, lowest 20% of the different input parameters is shown in blue values. The model runs (20%) with the lowest error are shown in green values in the comparison observations. The model runs (20%) with the largest error are shown in red values.

Run	Parameters					Comparison observations	
	K.Limestone <i>m/d</i>	K.Knip <i>m/d</i>	K.CLF <i>m/d</i>	K.Mid <i>m/d</i>	Recharge <i>m/d</i>	M.A.R. <i>m</i>	R.M.S.R. <i>m</i>
2	8.99	0.11	0.48	0.29	0.00060	153.82	216.14
3	0.31	0.11	0.86	0.40	0.00010	20.78	24.70
4	0.24	0.37	0.16	0.41	0.00022	119.64	147.87
5	0.33	0.19	1.91	0.27	0.00013	21.05	27.93
6	0.11	0.16	1.20	0.24	0.00019	75.71	107.21
7	0.19	0.07	6.49	0.32	0.00007	17.43	22.80
8	3.60	0.12	15.88	0.40	0.00041	16.08	25.37
9	5.84	0.42	0.13	0.28	0.00007	29.98	42.32
10	5.73	0.98	0.24	0.27	0.00020	46.91	70.16
11	0.33	0.84	0.61	0.40	0.00005	10.26	15.92
12	1.83	0.88	0.06	0.43	0.00043	359.16	579.45
13	3.48	0.60	6.37	0.21	0.00004	12.81	18.78
14	1.26	0.73	3.40	0.20	0.00053	41.12	53.42
15	2.93	0.50	2.50	0.40	0.00006	10.76	16.90
16	0.42	0.44	10.84	0.33	0.00019	21.16	29.34
17	23.17	0.35	0.48	0.24	0.00006	12.93	18.48
18	123.42	0.14	0.69	0.27	0.00020	34.64	46.50
19	757.64	0.30	0.17	0.43	0.00015	57.98	83.23
20	911.41	0.17	0.22	0.40	0.00025	93.61	134.90
21	513.15	0.11	19.04	0.25	0.00006	13.59	19.24
22	126.40	0.09	1.98	0.29	0.00020	14.90	19.95
23	767.05	0.36	4.80	0.36	0.00013	10.76	17.15
24	1844.74	0.05	1.98	0.40	0.00026	20.78	27.34
25	191.72	0.43	0.34	0.21	0.00005	13.42	19.29
26	1685.77	0.62	0.56	0.20	0.00033	46.38	61.91
27	446.77	0.49	0.08	0.31	0.00011	73.57	113.48
28	313.21	0.43	0.12	0.38	0.00036	173.52	268.56
29	80.24	1.03	16.39	0.26	0.00005	14.06	20.22
30	25.93	0.76	1.92	0.28	0.00053	29.48	39.32
31	70.63	0.95	4.01	0.30	0.00014	10.55	17.17
32	124.09	1.06	3.19	0.43	0.00053	18.80	24.26
Minimum	0.11	0.05	0.06	0.20	0.00004	10.26	15.92
Maximum	1844.74	1.06	19.04	0.43	0.00060	359.16	579.45
Average	259.38	0.45	3.45	0.32	0.00022	51.47	75.14

Table 8: Outflow calculations for all model runs. The minimum, maximum and average values are shown below. Highest 20% of the total outflow is shown in red values, lowest 20% of the total outflow is shown in blue values.

Run	Outflow			Outflow			Percentage	
	Total $m^3/d$	Sea $m^3/d$	Bays $m^3/d$	Total $m/d$	Sea $m/d$	Bays $m/d$	Sea %	Bays %
2	244260	132308	111952	0.87	0.47	0.40	54.2	45.8
3	39995	19014	20981	0.14	0.07	0.07	47.5	52.5
4	91481	55396	36085	0.33	0.20	0.13	60.6	39.4
5	54315	25065	29250	0.19	0.09	0.10	46.1	53.9
6	78507	35475	43032	0.28	0.13	0.15	45.2	54.8
7	28818	10410	18408	0.10	0.04	0.07	36.1	63.9
8	169126	69507	99620	0.60	0.25	0.36	41.1	58.9
9	26848	17059	9789	0.10	0.06	0.03	63.5	36.5
10	82906	53429	29477	0.30	0.19	0.11	64.4	35.6
11	20354	11855	8500	0.07	0.04	0.03	58.2	41.8
12	176003	116117	59886	0.63	0.42	0.21	66.0	34.0
13	16927	8368	8559	0.06	0.03	0.03	49.4	50.6
14	215487	112269	103217	0.77	0.40	0.37	52.1	47.9
15	23395	12429	10967	0.08	0.04	0.04	53.1	46.9
16	77291	31728	45563	0.28	0.11	0.16	41.0	59.0
17	24780	14495	10285	0.09	0.05	0.04	58.5	41.5
18	81255	42524	38732	0.29	0.15	0.14	52.3	47.7
19	61751	36619	25132	0.22	0.13	0.09	59.3	40.7
20	102355	58217	44139	0.37	0.21	0.16	56.9	43.1
21	23785	10893	12892	0.09	0.04	0.05	45.8	54.2
22	79973	38354	41619	0.29	0.14	0.15	48.0	52.0
23	51578	25547	26032	0.18	0.09	0.09	49.5	50.5
24	404630	248906	155724	1.45	0.89	0.56	61.5	38.5
25	18648	11024	7624	0.07	0.04	0.03	59.1	40.9
26	177337	107331	70006	0.63	0.38	0.25	60.5	39.5
27	44130	27155	16975	0.16	0.10	0.06	61.5	38.5
28	146316	89065	57251	0.52	0.32	0.20	60.9	39.1
29	22340	11057	11282	0.08	0.04	0.04	49.5	50.5
30	216757	122844	93914	0.77	0.44	0.34	56.7	43.3
31	58354	31664	26690	0.21	0.11	0.10	54.3	45.7
32	216287	119693	96593	0.77	0.43	0.35	55.3	44.7
Minimum	16927	8368	7624	0.06	0.03	0.03	36.12	34.03
Maximum	404630	248906	155724	1.45	0.89	0.56	65.97	63.88
Average	99225	55026	44199	0.35	0.20	0.16	53.82	46.18

## E Flow lines particles cross-section

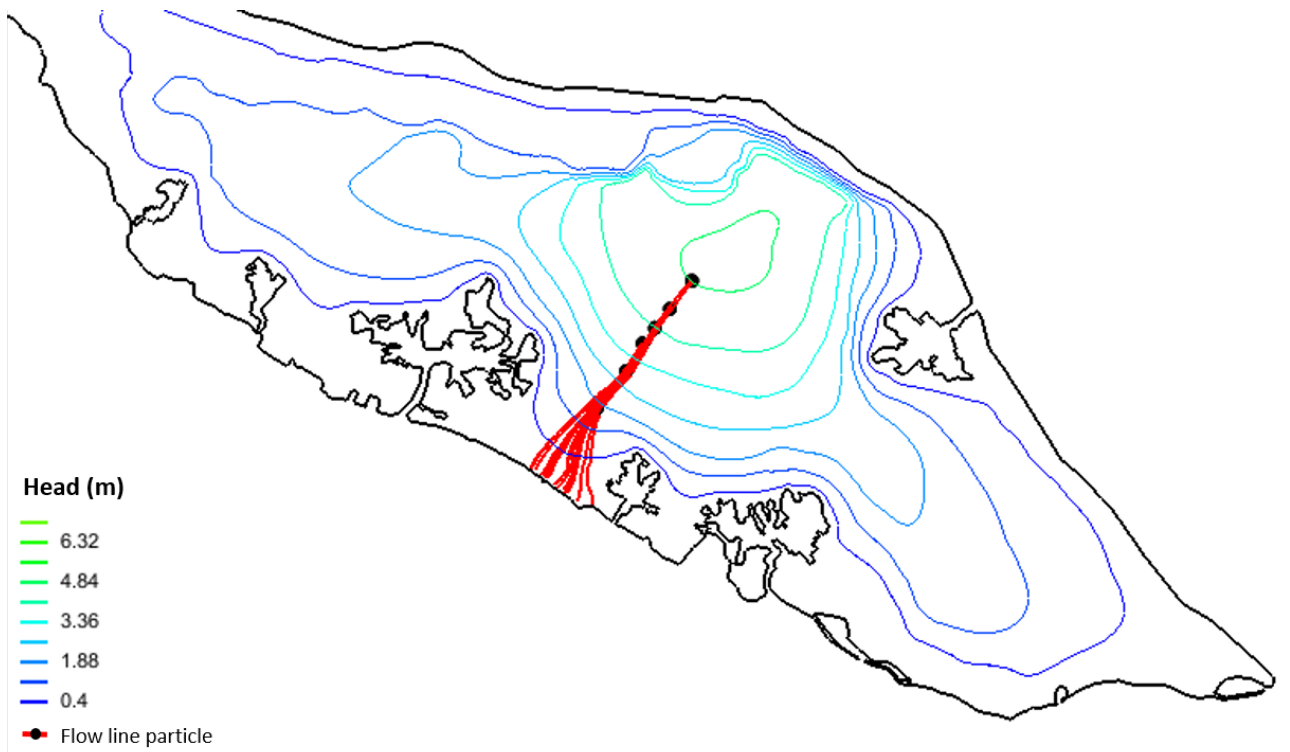


Figure 23: Flow lines of particles, these particles are located in the cross-section